Entry Flow Problem

of a

Liquid Body into a Suction Pipette

by

Anthony Kwok-Cheung Yeung

B.A.Sc., The University of British Columbia, 1983

A THESIS SUBMITTED IN PARTIAL FULFILLMENT OF

THE REQUIREMENTS FOR THE DEGREE OF

MASTER OF APPLIED SCIENCE

in

THE FACULTY OF GRADUATE STUDIES

DEPARTMENT OF PHYSICS

We accept this thesis as conforming to the required standard

THE UNIVERSITY OF BRITISH COLUMBIA

October 1987

In presenting this thesis in partial fulfilment of the requirements for an advanced degree at the University of British Columbia, I agree that the Library shall make it freely available for reference and study. I further agree that permission for extensive copying of this thesis for scholarly purposes may be granted by the head of my department or by his or her representatives. It is understood that copying or publication of this thesis for financial gain shall not be allowed without my written permission.

Department of ___*PHYSICS*___

The University of British Columbia
1956 Main Mall
Vancouver, Canada
V6T 1Y3

Date ___*October 14, 1987*___

ABSTRACT

The mathematical problem of the pipette aspiration of a liquid sphere is studied in the low Reynolds number limit. Two distinct models are proposed for the deforming body. They are: 1) a liquid droplet of constant viscosity, and 2) a viscoelastic cortex encapsulating an inviscid interior. These models represent energy dissipation distributed in the interior and on the surface of the body, respectively. Because the in-flow rates vary differently with the pipette size for the two models, this is suggested as a means of experimentally identifying the dominant region of viscous dissipation, and thus provide insight into the internal structure of the test sample.

For the droplet problem, the linear Stokes equations are solved in the interior of the deforming body. The solutions, for some specified stress boundary conditions on a sphere, can be expressed as infinite sums of Legendre polynomials.

In solving the surface flow problem, the complexities of the equations necessitate approximate solutions by computational means. A numerical procedure is developed which compares well with analytical results when the latter is available.

TABLE OF CONTENTS

LIST OF FIGURES

ACKNOWLEDGEMENT

I would like to thank Dr. Evan Evans, my thesis advisor, for introducing me to the field of scientific research, and for all the encouragement and support he has given me.

I. INTRODUCTION

Micropipette aspiration, which involves the manipulation and deformation of test samples with a suction pipette, has become an important technique in studying the mechanical properties of biological cells. Since its first application by Mitchison and Swann (1954) to their work on sea urchin eggs, the technique has developed extensively, particularly in the research area of red blood cell membranes (Rand and Burton, 1964; Evans, 1973; Evans and Hochmuth, 1977; Skalak et al., 1973). Recently, the micropipette technique has been adapted to the direct measurements of weak adhesive interactions between surfactant bilayers (Evans and Needham, 1986). All these applications involve measurements of static forces in equilibrium configurations. Time dependent behaviour of bodies (leukocytes) in a micropipette has also been investigated for small deformations (Schmid-Schonbein, et al., 1981; Chien and Sung, 1984). In these cases, the cell is treated as a "standard viscoelastic" material (see Fung, 1965), which, in essence, is a solid body with an elastic limit to deformation. The aim of this present work is to analyze the pipette aspiration of a liquid-like body in the context of continuum mechanics. The body of interest is assumed to be sufficiently large that it must deform upon entering the pipette. Models of the material properties of the body can then be used to predict its deformation and flow under the given external forces.

As the name implies, the theory of continuum mechanics requires the deforming body to have, even when its size is reduced to the limiting resolution of the experiment, a sufficient number of particles to enable a thermodynamic characterization of its macroscopic properties. The experiment that motivates this present analysis is the aspiration of human white blood cells (granulocytes) into micropipettes, as shown in figure 1, in an attempt to understand their rheological behaviour (Evans and Kukan, 1984). Here, the cells of interest are on the order of 10^{-3} cm in diameter - a length scale that is much larger than molecular dimensions. Ultrastructural evidence (Bessis, 1973; Schmid-Schonbein et al., 1980) has shown that the granulocyte is encapsulated in a plasma membrane that has a reservoir of excess surface area in the form of evenly distributed ruffles. This membrane, when in the flaccid state, is likely to offer little or no mechanical resistance to cell deformations (Evans and Skalak, 1980). Anchored to the underneath of the plasma membrane is a meshwork of densly packed, randomly oriented actin filaments (Southwick and Stossel, 1983; Amato et al., 1983). When stimulated to contract, these filaments are believed to provide for the cell's active locomotory. Because we are only interested in cells that are not "turned on", the cortical meshwork is considered here as a passive gel with its specific rheological properties. The small size of the actin filaments (8 nm in diameter) enables us to treat the gel as a continuum; moreover, because the filaments are randomly oriented on the cell surface, isotropy and
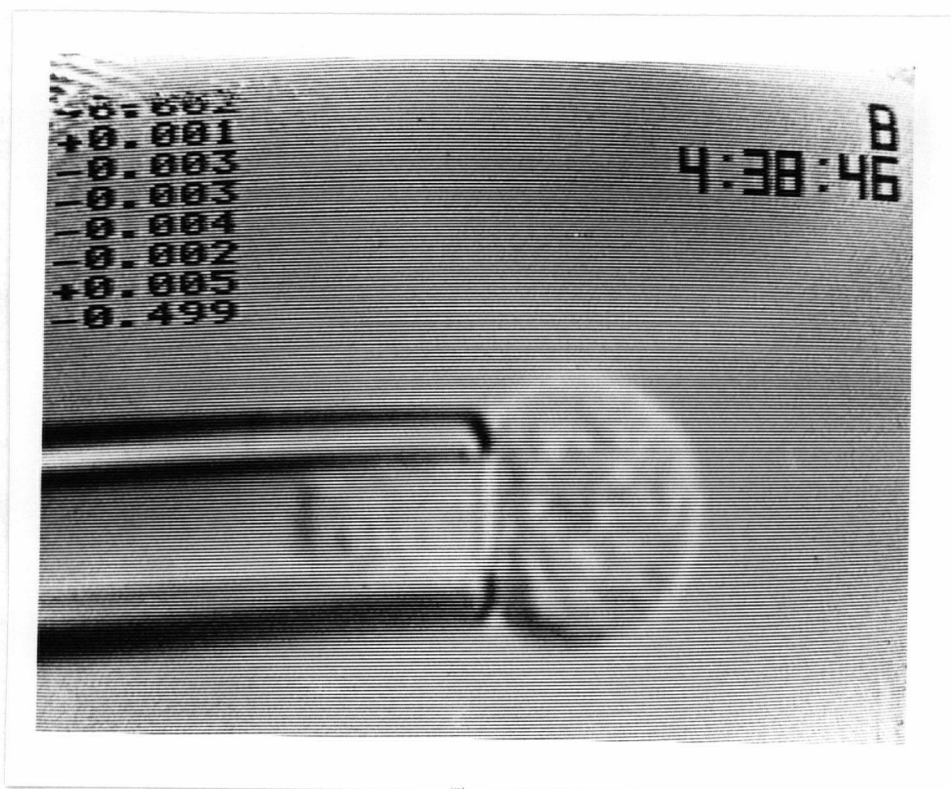
Figure 1: Aspiration of a human granulocyte at 23°C. The pipette inner radius is 2 micrometers and the suction pressure is 500 dynes/cm^2.

homogeneity in the surface plane (excluding the thickness dimension) can be assumed. In contrast to the cortex, the cell interior is highly heterogeneous in structure; that is, it contains organellar bodies like the nucleus and granules. This is a composite structure with each component being a continuum itself. To understand the overall property of this sturcture, we will model the cell interior as a three-dimensionally isotropic and homogeneous substance. In doing this, it is understood that the material properties assigned refer to the bulk of the interior, and should not be attributed to any one of the organellar components.

For the analysis in this thesis, the complicated structure of a granulocyte has been idealized as a three dimensionally isotropic substance surrounded by a two dimensionally isotropic gel. The next simplification is to identify the cell as essentially a liquid body. This is evidenced by the continuous flow of such cells into micropipettes when the suction pressure is in excess of a certain threshold value. This threshold pressure in turn is established by a cortical stress much like the interfacial tension between two liquids. The fact that the flow is continuous without any approach to static equilibrium indicates that no limiting elastic forces exist in the cell interior. Further, the cortical tension can be shown to be independent of deformation by lowering the suction pressure to the initial threshold. In such a case, the flow ceases and the aspirated projection of the cell inside the pipette remains

stationary.

In general, both the cortical shell and the interior may contribute to the viscous resistance to flow. The two limiting models proposed here are ones that have the viscous dissipation dominated by one of the regions, with the other region being essentially inviscid. In particular, the models are: 1) a liquid droplet with a constant viscosity, resulting in energy dissipation distributed throughout the interior, and 2) a viscous cortical shell encapsulating an inviscid fluid. The condition of volume conservation, as well as a cortical tension are incorporated into both models. Also, the viscous drag of the exterior aqueous solution on the cell is neglected because of the extremely slow response observed for cell entry into pipettes compared with the rapid in-flow of water at the same suction pressures (ie: flow rates that differ by a factor of 10^5). Because the dissipation of mechanical energy is volumetrically distributed in the former case and two dimensionally confined in the latter, the functional dependence of any flow related quantity (eg., the cell entry flow rate) on any characteristic length scale (eg., the pipette radius) should be distinctly different for the two models. These functional behaviours can be obtained by solving the above mentioned mechanical problems in the entire region that the cell occupies. The results will provide an experimenter with a means to discriminate the different viscous dissipation zones by performing aspiration tests with various sized pipettes.

Continuum mechanical analyses are composed of three independent and distinct developments. They are: 1) the quantitation of deformation and rate of deformation in relation to changes in the body's geometry; 2) the balance of forces within the body, as dictated by Newtonian mechanics; and 3) the modelling of the material properties of the substance. Knowledge of any two of these aspects can be used to predict the third one. For example, the deformation and rate of deformation of a body in response to controlled forces can be analyzed to give the material properties (eg: elastic and viscous coefficients). It is important to note that these three developments are formulated in terms of intensive quantities, ie: quantities that do not depend on the size of the sample. For instance, deformation is measured by strain, which is a dimensionless ratio of the material displacement to some initial length. Likewise, the distribution of forces is measured by its intensity (ie: on a per unit area basis) called stress. Material properties, which are coefficients relating the stresses and the deformations, are therefore based on local functions as well. The virtue of such formulations is that intrinsic properties of the substance can be defined independent of the nature of the experiment. In the following chapters, these three developments will be followed in arriving at the equations that govern the flow field. Analytical solutions to these equations are not available except for a few simplified cases. For the more general problem, we must be content with

approximate solutions by numerical means. These methods will also be discussed in the next chapters and the results will be presented.

II. PIPETTE ASPIRATION OF A DROPLET

The two models proposed in the introduction attributed the cell's stress bearing component to the interior and to the cortical region, respectively. To address the first problem, the pipette aspiration of a liquid droplet is analysed in this chapter. The droplet is to have a spherical initial geometry due to an interfacial tension, and the interior is modelled as an incompressible newtonian fluid. A similar problem is solved by Schmid-Schonbein et al. (1981) with the cell interior treated as a "standard viscoelastic solid". Because the authors have used the linearized strain tensor in their analysis, the results are valid only for small deformations.

Two simplifying assumptions are made here: 1) during aspiration, the portion of the body exterior to the pipette can be approximated as a spherical segment; and 2) viscous dissipation inside the pipette can be neglected. The first assumption is equivalent to the situation where the Laplace pressure (created by the interfacial tension) greatly exceeds the dynamic stress normal to the surface boundary. This criterion can be verified a posteriori from the final solution. The second approximation is introduced to represent the free-slip condition between the cell surface and the pipette wall (Evans and Kukan, 1984). By putting in proper boundary conditions, the present problem will have a unique solution in the form of a velocity field. We start our analysis by first

summarizing some equations relevant to the theory of continuum mechanics.

2.1: THE CREEPING MOTION EQUATIONS

Let x_i (i=1,2,3) be a coordinate system set up within the continuous body that locates every material point. If the velocity v_i (i=1,2,3) is continuous everywhere, then the rate of strain tensor is defined as

$$V_{ij} = \frac{1}{2} \left(\frac{\partial v_i}{\partial x_j} + \frac{\partial v_j}{\partial x_i} \right) \tag{2.1}$$

with the property that

$$\frac{d}{dt} (\Delta s^2 - \Delta s_o^2) = 2 \, V_{ij} \, \Delta x_i \, \Delta x_j \tag{2.2}$$[1]

Here, Δx_i is an instantaneous position vector connecting two points that are infinitesimally close, Δs is the absolute length of Δx_i, and Δs_o is the distance between the same two material points in the initial configuration. Because equation 2.2 involves only the difference between absolute lengths, the rate of strain tensor excludes all rigid body displacements and is therefore a true measure of deformation.

The trace of the rate of strain tensor represents volume

----

[1]The repetition of an index will imply summation with respect to that index over its range.

dilatation. Because the fluid is assumed incompressible in this case, V_{ii} vanishes. Expressed equivalently in terms of velocity components, the incompressibiliy condition is

$$\frac{\partial v_i}{\partial x_i} = 0 \qquad (2.3)$$

The stress vector $T_i(\mathbf{n})$ corresponding to a unit vector $\mathbf{n}$ is defined as follows: Consider a cross sectional area ΔA that is normal to $\mathbf{n}$. Let ΔF_i be the total force exerted on the positive side of ΔA (ie: the side on which $\mathbf{n}$ points outward). Obviously, the amount of force will decrease as the area shrinks. In the limit as ΔA vanishes, the stress vector is given by the ratio of ΔF_i to ΔA:

$$T_i(\mathbf{n}) = \lim_{\Delta A \to 0} \frac{\Delta F_i}{\Delta A} \qquad (2.4)$$

The stress tensor, σ_{ij}, is defined as the jth component of the stress vector on a plane whose normal is in the x_i direction:

$$\sigma_{ij} \equiv T_j(\mathbf{e}_i) \qquad (2.5)$$

Here, the unit vectors $\mathbf{e}_i$ are the basis set vectors.

For a newtonian liquid, the stress tensor is related to the rate of strain tensor by a proportionality constant:

$$\sigma_{ij} = -p\,\delta_{ij} + 2\,\eta\,V_{ij} \qquad (2.6)$$

η is called the coefficient of shear viscosity. The hydrostatic pressure p is introduced so that the trace of σ_{ij} remains non-zero. It can be viewed as a Lagrange multiplier associated with the incompressibility constraint.

The balance of forces within a continuum is expressed by the equation

$$\rho \frac{dv_i}{dt} = \frac{\partial \sigma_{ij}}{\partial x_j} + F_i \qquad (2.7)$$

where ρ is the mass density of the body, v_i the velocity, and F_i the body force per unit volume. Because the test samples (granulocytes) are freely suspended during experiment, there are no body forces (or rather they are negligible in comparison to the suction forces), and hence $F_i = 0$. The left hand side of equation 2.7 represents the inertial forces while the term $\frac{\partial \sigma_{ij}}{\partial x_j}$ for a newtonian fluid, as indicated in the last paragraph, represents the viscous forces. The ratio of the former to the latter is known as the Reynolds number (Landau and Lifshitz, 1982). From the characteristic sizes and flow rates of the micropipette experiments, the Reynolds number is estimated to have an upper bound of 10^{-6}, thus leaving the left hand side of equation 2.7 completely negligible. The equation of mechanical equilibrium for our purposes is therefore

$$\frac{\partial \sigma_{ij}}{\partial x_j} = 0 \qquad (2.8)$$

Combining equations 2.1, 2.3, 2.6, and 2.8, we arrive at the linear Stokes equation for creeping motions:

$$\vec{\nabla} \, p \; = \; \eta \, \nabla^2 \, \vec{v} \tag{2.9}$$

By taking the curl of equation 2.9 and using the vector identity

$$\vec{\nabla} \times \vec{\nabla} p \; = \; 0$$

the creeping motion equation can be further simplified to contain only the velocity term:

$$\nabla^2 \, (\vec{\nabla} \times \vec{v} \,) \; = \; 0 \tag{2.10}$$

By defining the quantity $\vec{\nabla} \times \vec{v}$ as the vorticity vector, we see that the creeping motion equations have been reduced to a homogeneous Laplace equation of vorticity.

2.2: PROBLEM FORMULATION AND SOLUTION

Equation 2.10 has to be satisfied at every point inside the droplet. In addition, proper boundary conditions have to be prescribed for the problem to be well posed. Consider the situation depicted in figure 2. Because of the body's geometry, it is natural to use spherical coordinates (ρ, θ). Here, the azimuthal angle ϕ drops out due to axisymmetry while θ, the polar angle, can be alternatively represented by its cosine:
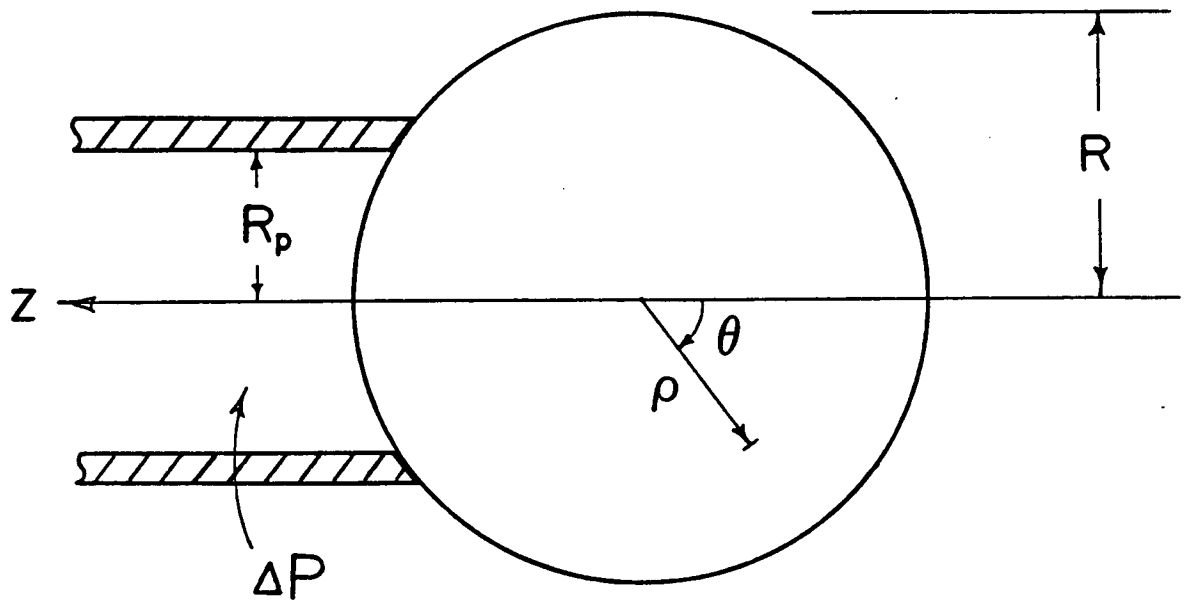
Figure 2: Definition of coordinates and various dimensions for the pipette aspiration problem. Note that there is a finite region of contact between the droplet and the pipette, as defined in eqn. 2.11.

$$\zeta = \cos \theta$$

In terms of ζ, the outer surface of the sphere can be divided into three regions that are subjected to different stresses. First, there is the part inside the pipette ($-1 < \zeta < \zeta_p$) that experiences a suction pressure ΔP. The region in contact with the pipette ($\zeta_p < \zeta < \zeta_p + \epsilon$) is under a uniform compressive load λ/ϵ (being a small quantity), while the remaining spherical portion ($\zeta_p + \epsilon < \zeta < 1$) is stress free. The magnitude of λ can be related to ΔP by requiring the total axial force on the body be zero. The externally applied normal stresses are collectively called $\alpha(\zeta)$ such that

$$\alpha(\zeta) = \begin{cases} \Delta P & ; \quad -1 < \zeta < \zeta_p \\ -\lambda/\epsilon & ; \quad \zeta_p < \zeta < \zeta_p + \epsilon \\ 0 & ; \quad \zeta_p + \epsilon < \zeta < 1 \end{cases} \qquad (2.11)$$

with ΔP and λ both positive quantities. The stress boundary conditions are therefore

$$\sigma_{\rho\rho}(\zeta)\Big|_{\rho=R} = \alpha(\zeta) \qquad (2.12)$$

for the normal stress, and

$$\sigma_{\rho\theta}(\zeta)\Big|_{\rho=R} = 0 \qquad (2.13)$$

for zero tangential stress. In an axisymmetric problem, the quantities $\sigma_{\rho\rho}$ and $\sigma_{\rho\theta}$ are the only possible non-zero stresses

on the coordinate surface $\rho = R$.

The solution to the Laplace equation for vorticity (equation 2.10) can be expressed as infinite sums of polynomials in ρ and angular harmonics in ζ, as developed by Happel and Brenner, 1973 (see appendix A). By matching boundary conditions 2.12 and 2.13 to the general solutions of equation 2.10, the final form of the solution is obtained. In particular, on the boundary $\rho = R$, they are

$$v_\rho(\zeta) = -v_z^{\,0}\,\zeta - \sum_{n=3}^{\infty} \frac{(n-1)(2n-1)}{2(n-2)(2n^2+1)}\,R\,a_n\,P_{n-1}(\zeta) \qquad (2.14a)$$

$$v_\theta(\zeta) = v_z^{\,0}\sin\theta + \sum_{n=3}^{\infty} \frac{3n(n-1)}{2(n-2)(2n^2+1)}\,R\,a_n\,\frac{I_n(\zeta)}{\sin\theta} \qquad (2.14b)$$

$$p(\zeta) = -\frac{\Delta P(1+\zeta_p)(1+\zeta_p+\epsilon)}{2(2\zeta_p+\epsilon)} + \eta\sum_{n=3}^{\infty} \frac{n(2n+1)}{2n^2+1}\,a_n\,P_{n-1}(\zeta) \qquad (2.14c)$$

where $P_n(\zeta)$ is the Legendre polynomial of degree n, and $I_n(\zeta)$ the Gegenbauer polynomial given by

$$I_n(\zeta) \equiv \frac{P_{n-2}(\zeta) - P_n(\zeta)}{2n - 1} \qquad (2.15)$$

with the degenerate cases defined as

$$I_0(\zeta) \equiv P_0(\zeta) = 1 \;\; ; \;\; I_1(\zeta) \equiv -P_1(\zeta) = -\zeta \qquad (2.16)$$

The condition that $v_\rho = 0$ at the point where the sphere touches the pipette is satisfied by superimposing an axial velocity

onto the series solutions. The Legendre coefficients a_n are functions of ΔP, η, and geometry. The expression for a_n, as well as a derivation of equations 2.14 are given in appendix A.

2.3: SURFACE TENSION EFFECTS

The normal stress boundary condition, equation 2.11, does not include any interfacial tension contribution. Adding the Laplace pressure term $-2\bar{T}_o/R$ ($\bar{T}_o$ being the interfacial tension with units of force/unit length) to the right hand side of 2.11 in fact leaves the final expression for a_n, and hence the velocity field, unaltered. This is because the geometry of a droplet (ie: sphere) is the equilibrium configuration created by the interfacial forces. The velocity fields in equations 2.14, representing the balance of viscous stresses against forces that deform the sphere, are therefore independent of $\bar{T}_o$. Any deviation from this equilibrium shape, however, will be resisted by the interfacial tension. By calculating this resistance to shape changes, it is shown that despite of the surface tension effect, the results from section 2.2 are still useful if the quantity ΔP is interpreted as a pressure in excess of some thershold value.

Consider the aspiration of a liquid droplet that has a constant interfacial tension $\bar{T}_o$. The pressure P_{eq} required to hold the droplet at <u>static</u> equilibrium at a projected length d is calculated, keeping the volume of the drop fixed. Figure 3
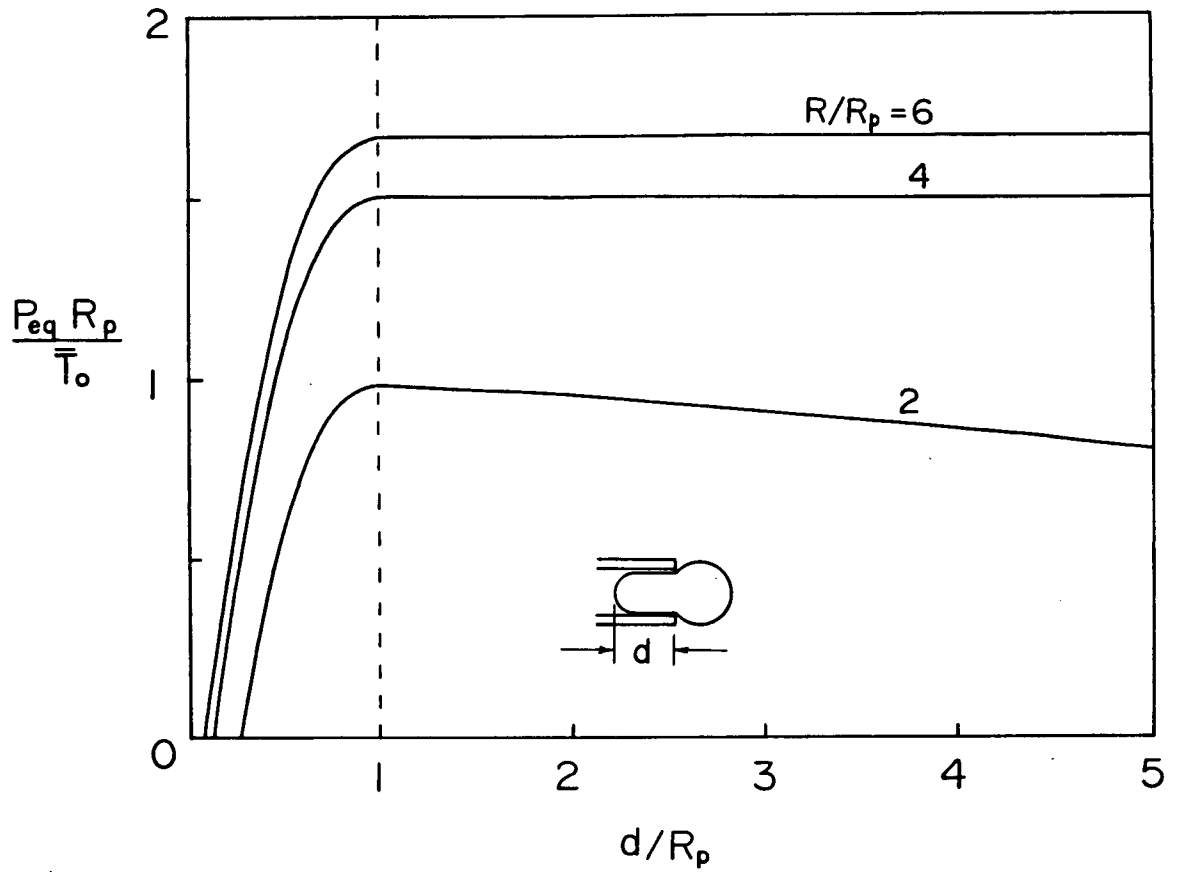
Figure 3: Suction pressure required to hold a liquid droplet at static equilibrium versus the projected length for different initial cell sizes.

shows the plot of the dimensionless pressure, $P_{eq}R_p/\bar{T}_o$, as a function of d/R_p for various cell sizes. The common feature to all these curves is the steep rise in pressure for projections less than one pipette radius (ie: before a hemi-spherical cap is formed in the pipette), followed by an essentially constant or even decreasing pressure level. The pressure required to form the hemispherical cap can be calculated from the equation

$$\hat{P} = 2\,\bar{T}_o\,(\frac{1}{R_p} - \frac{1}{R}) \qquad (2.17)$$

This is the threshold that must be exceeded for flow to commence. For pressures above the threshold, the amount in excess of $\hat{P}$ (approximately) is the effective pressure that is balanced against the viscous forces. Assuming there is no pressure drop along the aspirated length (the plug flow assumption), this excess pressure is just the quantity ΔP in equation 2.11. To be exact, we write

$$\Delta P = P - \hat{P} \qquad (2.18)$$

where P is the applied suction pressure. With this new interpretation of ΔP, the velocity fields (eqns. 2.14a & 2.14b) remain unchanged, while the quantity $p(\theta)$ in equation 2.14c should be replaced by

$$p(\theta) - 2\bar{T}_o/R \ ,$$

which is the correction for the Laplace pressure.

2.4: RESULTS AND DISCUSSION

The volumetric flow rate into the pipette is derived from the relation

$$Q = - 2\pi R^2 \int_0^{\theta_p} v_\rho \sin\theta \, d\theta \qquad (2.19)$$

where θ_p is the value of θ at the pipette entrance. Equation 2.19 can be integrated using the formula

$$\int_0^\zeta P_n(x) \, dx = - I_n(\zeta)$$

to obtain

$$Q = \pi R_p^2 v_z^o - \sum_{n=3}^\infty \frac{\pi R^3 (n-1)}{(n-2)(2n^2+1)} a_n \left[P_n(\zeta_p) - P_{n-2}(\zeta_p) \right] \qquad (2.20)$$

The rate of growth of the projection inside the pipette is calculated from the volumetric flow rate:

$$Q \equiv \pi R_p^2 \dot{L} \qquad (2.21)$$

All quantities in the above equations are made dimensionless by scaling with R_p, η, and ΔP. Figure 4 shows a plot of the dimensionless rate of entry as a function of the pipette radius. As the sphere radius approaches infinity, the dimensionless flow rate, $\dot{L} \eta / (\Delta P R_p)$, has a limiting value of 0.25. The similar problem of viscous flow from an infinite half-space into an orifice is solved by Happel & Brenner (1973) and Torzeren et al. (1984) with different velocity boundary conditions along the
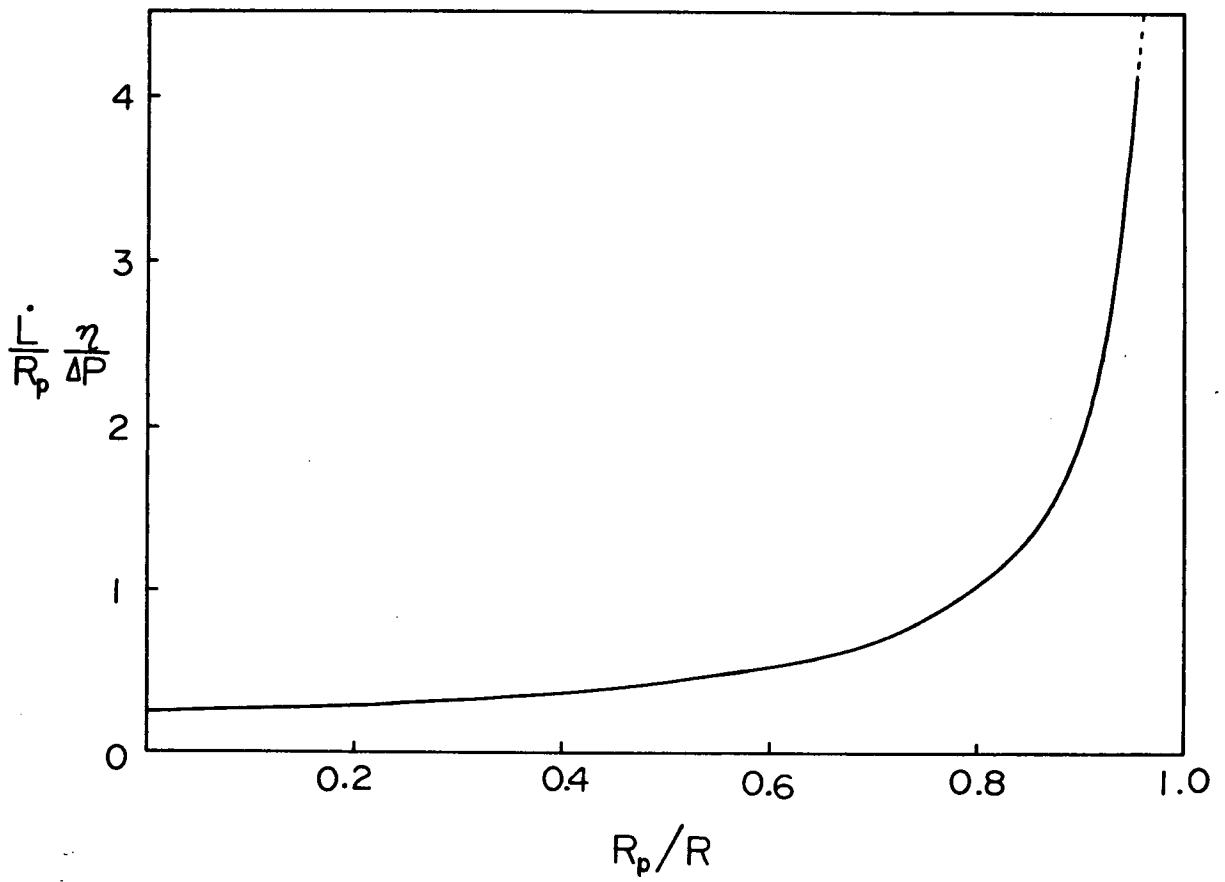
Figure 4: The dimensionless flow rate as a function of the pipette radius for a newtonian liquid droplet.

septum: the former used the no slip boundary condition while the latter assumed the velocity be driven by a radially convergent membrane (ie: radial velocity proportional to 1/r). Because the present problem involves the free-slip boundary condition (eqn. 2.13), we expected the flow rate to be greater than the no-slip case, and less than that for the membrane driven flow. Indeed, with the same scaling as used above, the dimensionless flow rates are respectively $\frac{2}{3\pi}$ (0.212) and 1/2.

On the surface ρ = R, our initial assumption of negligible normal stress in comparison to the Laplace pressure (created by the interfacial tension) can now be verified. Using equation 2.14c, the dynamic pressure is calculated on the surface of the sphere. The result, as shown in figure 5, is that there is no appreciable pressure difference (relative to the external medium) on the segment exterior to the suction pipette. This implies that all the pressure drop must be concentrated in a small region at the orifice entrance where the velocity gradients are large.
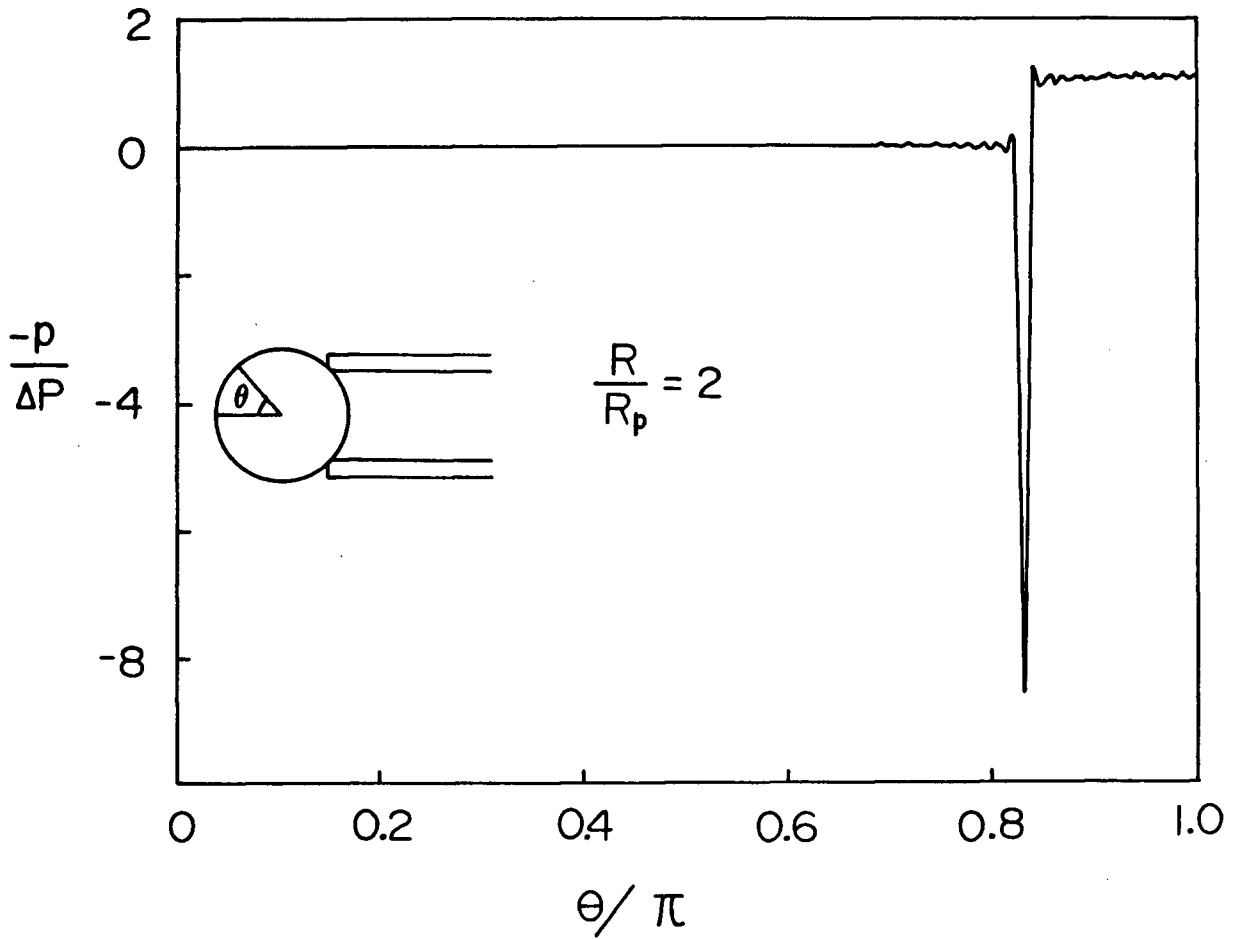
Figure 5: The dimensionless hydrostatic pressure vs. the curvilinear distance on the surface ρ = R. The sharp drop in pressure at θ/π = 0.83 corresponds to the pipette contact region.

III. TWO-DIMENSIONAL MEMBRANE MECHANICS

The theory of two-dimensional thin shell mechanics has been
extensively developed by Evans and Skalak (1980), which forms
the theoretical basis of this chapter. The principles will be
applied to the axisymmetric problem of the pipette aspiration of
a cortical shell. The fluid inside the cell is assumed to be
inviscid and incompressible, resulting in a uniform internal
pressure. Material properties of the cortex, on the other hand,
can be quite general. In addition to having an isotropic
interfacial tension that accounts for the cell's spherical
shape, the cortex can also be "viscoelastic". This is a general
description of a family of models that are combinations of two
basic idealizations: the linear elastic body and the linear
viscous body. These will be discussed in more details in later
sections. Because of the sharp bend observed for aspirated
cells at the edge of the pipette entrance (see figure 1), we
anticipate a negligible bending rigidity in the cortical layer.
As such, the problem is reduced to consideration of forces that
act only in the surface plane. The development of this chapter
will thus be based on two simplifications: axisymmetry and the
neglect of bending moments.

In contrast to a thin sheet of rubber, for example, which
has small scale structure even across the thickness dimension, a
two-dimensional membrane can have isotropy characterized only in
the surface plane. Though it may seem unusual as an engineering

material, such a concept finds itself quite common in the field of biological membranes. As an example, consider the fundamental component of the biological cell membrane - the lipid bilayer. It is composed of two layers of lipid mosaic as shown in figure 6. Because each lipid molecule only occupies an area of approximately 100 $\overset{\circ}{A}^2$, on a cellular scale (ie: micrometers), the surface plane of the bilayer can be considered a continuum. Across the thickness, however, there are precisely two molecules. The principles of continuum mechanics are obviously invalid in this dimension. This anisotropic structure is reflected in the mechanical properties of the bilayer membrane, as measured by Kwok and Evans (1981). For example, bilayers above the acyl chain crystallization temperature exhibit a very strong static resistance to area expansions, but has no such resistance to shape changes under constant area. These conflicting values of static rigidities are uncharacteristic of a thin membrane that is three-dimensionally isotropic. It can however be rationalized by recognizing the discontinuity in the third dimension.

The assumption of a two-dimensional membrane is a generalization rather than a restriction. In general, deformations of a thin sheet can be expressed as a superposition of two fundamental modes: area dilatation and in-plane shear. The resistance of the material to these two modes of deformation are expressed numerically as the "moduli" of elasticity (or the moduli of viscosity for resistance to rates of deformation).
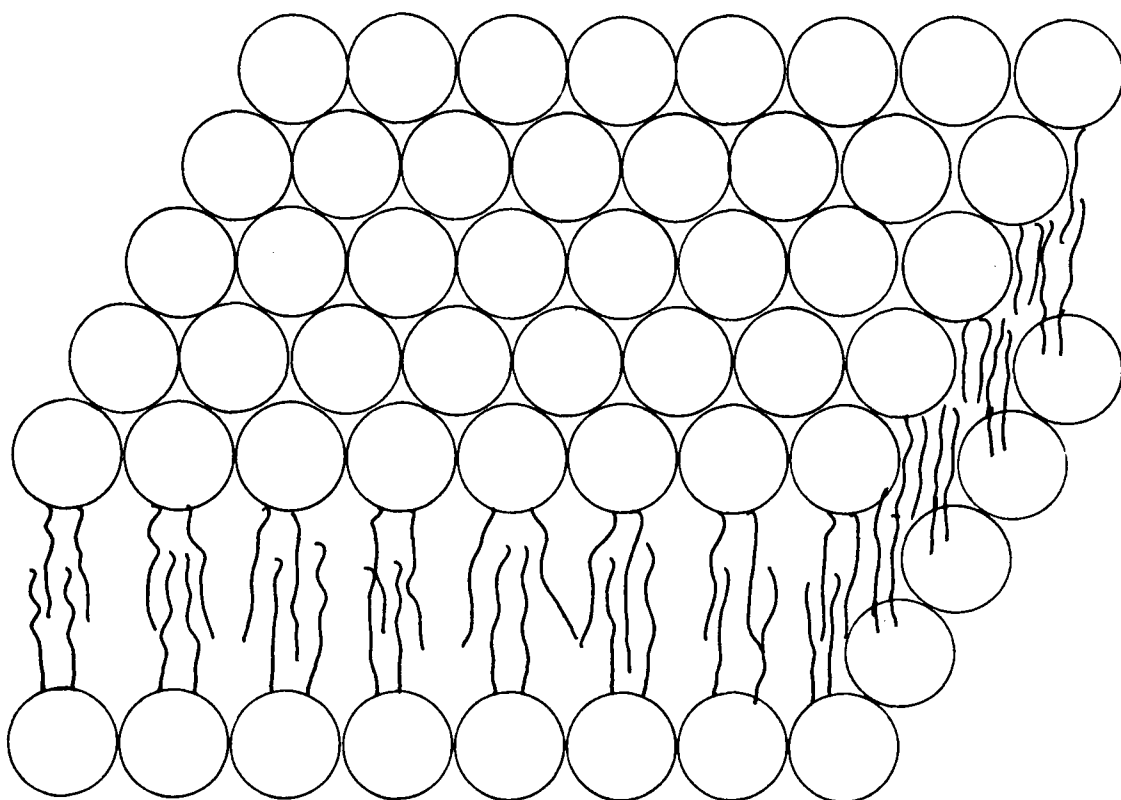
Figure 6:   Schematic illustration of a section of the lipid
            bilayer, which comprises of two layers of lipid
            molecules arranged in two-dimensional arrays.

For a three dimensionally isotropic shell material, the moduli associated with the two modes of deformation are uniquely related whereas in the case of a two-dimensional material, this restriction is removed and the two moduli can be completely independent of each other (see Evans, 1973 for a more detailed discussion).

The first parts of this chapter will be devoted to the theoretical aspects of two-dimensional thin shell mechanics. A numerical algorithm that applies the principles to the pipette aspiration of a cortical shell will then be discussed.

3.1: ANALYSIS OF STRAIN

To analyze the deformation of a thin membrane, we conceptualize the initial (undeformed) surface as a grid of many elemental squares, with each region small enough that locally it can be treated as a flat surface. By comparing the size and shape of each instantaneous element to its initial configuration, we can have complete information on the body's deformation field. Each differential element can be oriented so that a square maps simply into a rectangle in the deformed state. This especially convenient orientation is said to be in the principal coordinate system. For an axisymmetric surface (ie: a surface generated by revolving a meridian curve about an axis) with deformations symmetric about the same axis, the principal coordinates are immediately given - they are in the

meridional and the azimuthal directions.

Two quantities are needed to relate the instantaneous rectangle to the initial square. The simplest are the extension ratios λ_m and λ_ϕ, which are the ratios of the deformed length to the original length in the meridional and the azimuthal directions, respectively. In the case of axisymmetry, any quantity can be expressed as a function of one spatial variable alone - namely the curvilinear position s of a material point along the meridian. This variable in turn can be uniquely related to the initial curvilinear distance of the same material point, s_o. In this manner, the extension ratios are given by

$$\lambda_m(s_o) = \frac{ds}{ds_o} \tag{3.1}$$

$$\lambda_\phi = \frac{r}{r_o} \tag{3.2}$$

where $r(s_o)$ and $r_o(s_o)$ are respectively the radial distances from the axis of symmetry in the instantaneous and the initial configurations.

Although the extension ratios provide a complete description of the strain field, there are other deformation variables that have more relevance to the physics of the membrane material. Consider the uncoupling of a general deformation into the two fundamental modes: 1) expansion or contraction without shape changes; and 2) deformation at constant area. Figure 7 shows
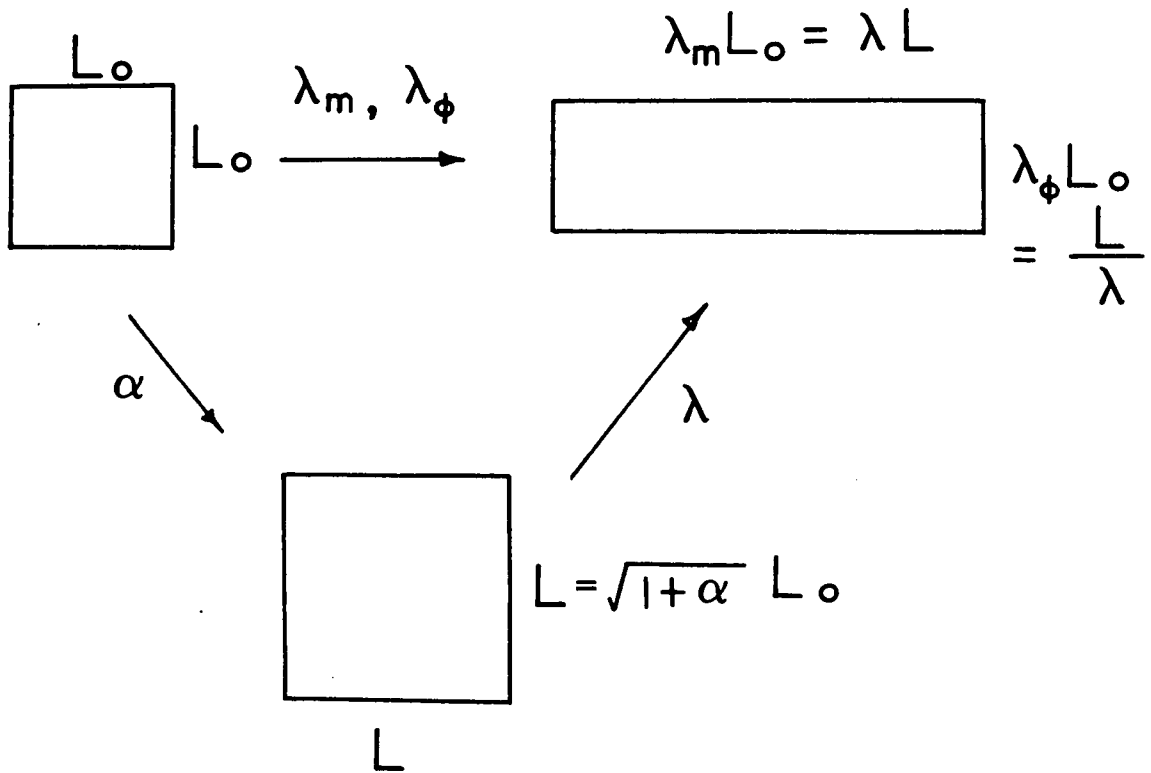
Figure 7: The uncoupling of a general deformation into the two independent modes.

such a case in the principal coordinate system. The actual deformation that involves the two extension ratios can be broken down into two steps - the first one characterized by α , the fractional area change, and the second one by λ , which measures the amount of extension. These deformation variables can easily be related to the extension ratios:

$$\alpha = \lambda_m \lambda_\phi - 1 \qquad (3.3)$$

$$\lambda = (\lambda_m / \lambda_\phi)^{\frac{1}{2}} \qquad (3.4)$$

The two variables, α and λ , form a set of linearly independent functions (with respect to λ_m and λ_ϕ) that completely specifies the geometric features of the deformation. Likewise, the time rates of deformation can be seperated into the same two modes. In an Eulerian formulation (ie: with the instantaneous coordinates as the reference geometry), the rate of deformation variables are not the time derivatives of α and λ , but of their logarithms (see Evans and Skalak,1980):

$$V_\alpha = \frac{d}{dt} \ln(1+\alpha) \qquad (3.5)$$

$$V_s = \frac{d}{dt} \ln \lambda \qquad (3.6)$$

Thus, the deformation and rate of deformation of an axisymmetric body is quantitated in terms of four intensive variables - each of which can be expressed as a function of the

initial curvilinear distance s_o.

3.2: BALANCE OF FORCES IN A TWO-DIMENSIONAL MEMBRANE

In Newtonian mechanics, the sum of all forces and the sum of all moments acting on a body must be zero in the absence of accleration. As mentioned earlier, the bending moments in the cortical layer is assumed negligible in this study. The membrane force resultants therefore must act tangent to the plane of the surface. For an axisymmetric problem, these forces are expressed in terms of two tension resultants, T_m and T_ϕ, as shown in figure 8a. These are intensive quantities defined as the force per unit length in the meridional and the azimuthal directions respectively. From the characteristic sizes and flow rates of the micropipette experiment, inertial effects are negligible in comparison to other forces. Thus, mechanical equilibrium requires the balance of the internal forces in the thin shell (eg: elastic and viscous forces) against the applied stresses (eg: the suction pressure). In an axisymmetric configuration, the equilibrium equations for a membrane are (see Evans and Skalak, 1980)

$$\frac{\partial}{\partial s} (r\, T_m) - T_\phi \frac{\partial r}{\partial s} + \sigma_s = 0 \qquad (3.7a)$$

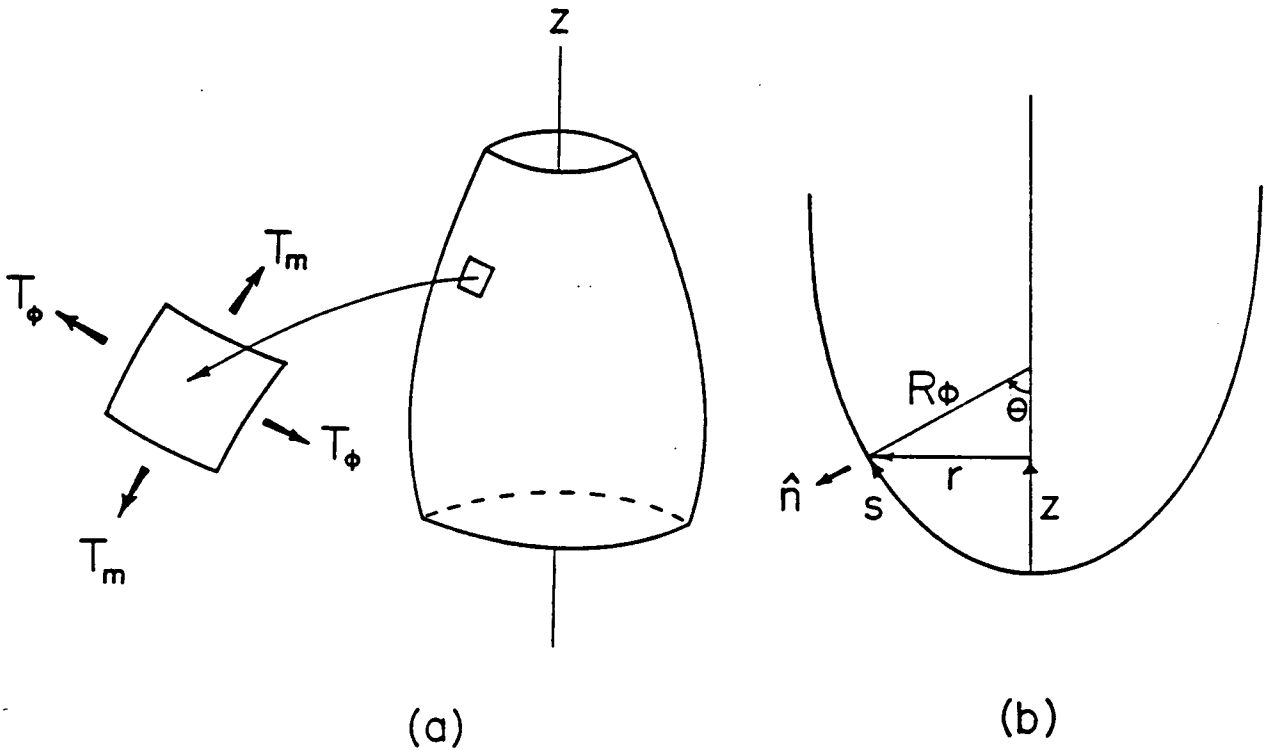$$\frac{T_m}{R_m} + \frac{T_\phi}{R_\phi} = \sigma_n \qquad (3.7b)$$

Figure 8: The tension resultants and coordinate variables
are illustrated for an axisymmetric geometry.
(a) The tension resultants act only in the
meridional and azimuthal directions, which are
also the principal directions.
(b) Definition of the coordinate variables. R_m,
the meridional curvature, is not shown.

All variables in equations 3.7 are as defined in figure 8. Note that σ_n and σ_s are the externally applied stresses that have dimensions of force per unit area (unlike the tension resultants, which have dimensions of force/length). The quantities R_m and R_ϕ are the radii of curvature in the meridional and azimuthal directions. They can be related to the coordinate variables by

$$R_m = \frac{d\theta}{ds} \tag{3.8}$$

$$R_\phi = \frac{r}{\sin \theta} \tag{3.9}$$

where θ is defined as the angle between the outward normal vector and the axis of symmetry. It follows from this definition that

$$\sin \theta = \frac{dz}{ds} \tag{3.10}$$

$$\cos \theta = \frac{dr}{ds} \tag{3.11}$$

Equations 3.7 are the differential equations of mechanical equilibrium. It is also possible to cumulate the axial component of the external stresses and equate to the meridional tension, resulting in a set of integrated equations which are alternatives to 3.7. They are

$$T_m = \frac{F_z}{2\pi \, r \, \sin \theta} \tag{3.12a}$$

$$T_\phi = \frac{r}{\sin \theta} (\sigma_s - \frac{F_z}{2\pi \, r \, \sin \theta} \frac{d\theta}{ds}) \qquad (3.12b)$$

where

$$F_z(s) \equiv 2\pi \int_0^s r \, ds \, (\sigma_n \cos \theta - \sigma_s \sin\theta) \qquad (3.13)$$

Equations 3.12 are valid for an axisymmetric geometry with the curvilinear coordinate s originating from a pole. They can be shown to be equivalent to 3.7. Because the fluids both interior and exterior to the cortical shell are assumed inviscid, there can be no shear stresses on the membrane, and hence $\sigma_s = 0$. Also, for the same reason, there is a uniform pressure σ_n inside the cortical shell (relative to the external medium) that is independent of the coordinate s. With these simplifications, we can readily evaluate the axial force in equation 3.13 and substitute into 3.12. The equations of equilibrium then become

$$\epsilon_\alpha \equiv 4\overline{T} - \sigma_n \frac{r}{\sin \theta} (3 - \frac{r}{\sin \theta} \frac{d\theta}{ds}) = 0 \qquad (3.14a)$$

$$\epsilon_s \equiv 4\overline{T} - \sigma_n \frac{r}{\sin \theta} (\frac{r}{\sin \theta} \frac{d\theta}{ds} - 1) = 0 \qquad (3.14b)$$

where $\overline{T}$ and T_s are respectively the isotropic and deviatoric tensions defined as

$$\overline{T} \equiv \tfrac{1}{2} (T_m + T_\phi) \qquad (3.15)$$

$$T_s \equiv \frac{1}{2}(T_m - T_\phi) \qquad (3.16)$$

The above equations of equilibrium express the balance of forces (an extrinsic quantity) in a thin membrane that has no bending rigidity. The equations have to hold regardless of the structure of the membrane. For example, the questions of whether the material is isotropic, or whether it is solid or liquid, are irrelevant.

3.3: CONSTITUTIVE RELATIONS

Any relation that describes the property of a material can be called a constitutive relation. In this present work, we are interested in mathematical functions that relate the intensive deformation variables (α, λ) to the intensive stress variables ($\bar{T}$, T_s) at constant temperature. Much information about the material is revealed in these relations. For instance, an elastic solid is one that has conservative internal forces (ie: forces that can be represented as the gradient of a scalar function). Elastic stresses can only depend on the body's deformation and not on its time rate. A liquid, on the other hand, is characterized by its inability to sustain shear stresses in a state of rest. In the process of deforming, however, there is inevitably internal molecular friction and structural changes that appear macroscopically as a resistance to flow. The stresses of a viscous liquid will therefore depend only on the rate of deformation variables.

The simplest way to model solid and liquid behaviours is to take the first order approach. For an elastic solid undergoing isothermal deformations, the mechanical work done can be shown to be equivalent to the change in the Helmholtz free energy of the body (the body is considered here as a closed system). It follows from the definition of mechanical work that the stresses are the derivatives of the Helmholtz free energy with respect to the corresponding strain variables. To obtain a first order stress-strain relation, the free energy is written as a Taylor expansion in terms of the deformation variables up to the quadratic terms (see Evans and Skalak, 1980). In this manner, the elastic stresses are given by

$$\bar{T}^e = \bar{T}_o + K \alpha \qquad (3.17)$$

$$T_s^{\ e} = \tfrac{1}{2} \mu \ (\frac{\lambda^2 - \lambda^{-2}}{1 + \alpha}) \qquad (3.18)$$

where the superscripts "e" denote elastic stresses. $\bar{T}_o$ is a constant isotropic tension which may arise from interfacial effects. K and μ are respectively the isotropic and shear moduli of elasticity. For a three dimensionally isotropic material, it can be shown that $K = 3\mu$, whereas for a material that is anisotropic in the thickness dimension, these two moduli are completely unrelated.

The viscous forces in a liquid arise from internal friction

and heat dissipation that are thermodynamically irreversible. Because of their complexities, these non-conservative forces are best described by phenomenological relations. To first order, such relations are

$$\bar{T}^V = \kappa \ V_\alpha \tag{3.19}$$

$$T_s{}^V = 2 \ \eta \ V_s \tag{3.20}$$

where the superscripts "v" denote viscous stresses. κ and η are respectively the isotropic and shear moduli of viscosity. Like the elastic solid, the moduli of viscosity are related by a 3:1 ratio for a three-dimensionally isotropic material, and are unrelated in the two-dimensional case.

In reality, most materials do not exhibit purely elastic or purely viscous characteristics. The two first order models introduced can be thought of as the idealized "extremes" of material behaviours: 1) the elastic solid that is capable of instantaneous deformation when subject to impulsive forces, with mechanical work fully recovered upon unloading, and 2) the viscous liquid that has a finite rate of deformation and with no tendency of returning to the initial configuration upon removal of external forces. Work done by a viscous liquid is completely irrecoverable. These two first order idealizations can be combined to model "intermediate" cases of mixed behaviours. Although in principle there can be an infinite number of

combinations, we will introduce three models that account very
well for most material behaviours. The first two models are
illustrated metaphorically in figure 9, using a spring to denote
the elastic component and a piston to denote the viscous
counterpart. In the first case, the so-called Voigt model, an
elastic element is placed in parallel with a viscous element to
represent solids that have appreciable internal energy
dissipation. Although the material is capable of returning to
the original configuration upon removal of external forces
(which characterizes it as a solid), the load-unload curve will
always show hysteresis due to viscous dissipation. For this
model, the total force is the sum of the two contributions:

$$\overline{T} = \overline{T}^e + \overline{T}^v \tag{3.21}$$

$$T_s = T_s{}^e + T_s{}^v \tag{3.22}$$

and the deformation is by definition common to both elements:

$$\alpha = \alpha_e = \alpha_v \tag{3.23}$$

$$\lambda = \lambda_e = \lambda_v \tag{3.24}$$

Unlike the Voigt material, which can be considered as
essentially a solid, there are other substances which show
internal stress relaxation mechanisms. These materials are
characterized by two observations: 1) an elastic response to
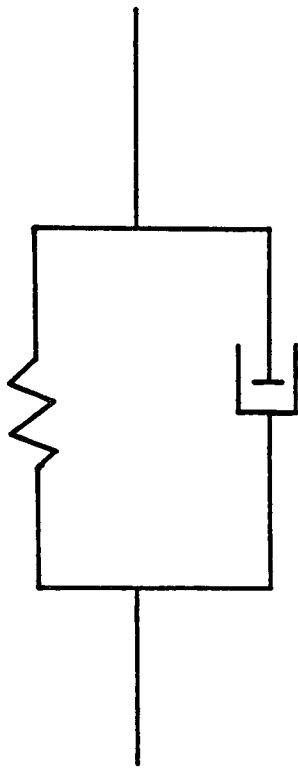
Figure 9: Metaphorical representations of viscoelastic models using combinations of springs (elastic component) and dashpots (viscous component). (a) the Voigt model; (b) the Maxwell model.

impulsive forces, and 2) liquid flow behaviour under constant shear stresses. Such materials can adequately be described by a first order Maxwell model, as shown in figure 9b. Because of the serial coupling, the stresses are common to both elements:

$$\overline{T} = \overline{T}^e = \overline{T}^v \qquad (3.25)$$

$$T_s = T_s{}^e = T_s{}^v \qquad (3.26)$$

and the total rate of deformation is defined as the sum of the two individual parts:

$$V_\alpha = V_\alpha{}^e + V_\alpha{}^v \qquad (3.27)$$

$$V_s = V_s{}^e + V_s{}^v \qquad (3.28)$$

For the general first order constitutive relations given by 3.17 to 3.20, the rate of deformation variables for a Maxwell model can be expressed in terms of the stresses as

$$\frac{\partial \ln(1+\alpha)}{\partial t} = \frac{1}{\sigma} \frac{\partial \overline{T}}{\partial t} + \frac{\overline{T}}{\kappa} \qquad (3.29)$$

$$\frac{\partial \ln \lambda}{\partial t} = \frac{1}{2(T_s{}^2 \sigma^2 + K^2 \mu^2)^{\frac{1}{2}}} \left(T_s \frac{\partial \overline{T}}{\partial t} + \sigma \frac{\partial T_s}{\partial t} \right) + \frac{T_s}{2\eta} \qquad (3.30)$$

where

$$\sigma \equiv \overline{T} - \overline{T}_o + K \qquad (3.31)$$

The ratio of the viscous modulus to the elastic modulus in a
Maxwell model define a relaxation time τ that determines its
semi-solid behaviour. In particular, the model predicts an
elastic response to forces that are applied for a time duration
much shorter than τ , and a liquid response to durations that
are large compared to τ . In the limit that the relaxation time
approaches zero, the Maxwell model becomes an ideal liquid.

While the Maxwell body is characterized by a time constant
related to its internal stress relaxation, there is another
class of semisolid - the viscoplastic material (or the Bingham
material) that is characterized by a stress magnitude called the
yield shear. In this case, the body behaves elastically under
stress levels below the yield shear. Beyond this point, the
material begins to show liquid flow with the rate of deformation
proportional to the amount of stress in excess of the yield.
The constitutive relation for a two dimensionally incompressible
ideal plastic is

$$T_s = \frac{1}{2} \mu (\lambda^2 - \lambda^{-2}) \qquad ; \qquad |T_s| < \hat{T}_s \qquad (3.32a)$$

$$|T_s| - \hat{T}_s = 2 \eta |V_s| \qquad ; \qquad |T_s| > \hat{T}_s \qquad (3.32b)$$

where $\hat{T}_s$ is the yield shear which is a positive quantity. In
equation 3.32b, the rate of deformation V_s is to have the same
sign as T_s. The elastic coefficient μ can be made very large to

account for the negligible yield strain in most plastic
materials. In the limit the yield shear vanishes, the ideal
plastic becomes a liquid.

3.4: THE LINEAR QUASI-ELASTIC SOLUTION

In the previous sections, we have introduced equations that
describe the time evolution of a two dimensional membrane under
external stresses. In particular, the balance of mechanical
forces, as expressed in equations 3.14, must be satisfied. The
quantities $\bar{T}$ and T_s in these equations are characteristic of the
material model chosen, with the constitutive relations as
outlined in equations 3.17 to 3.32. The deformation and rate of
deformation variables in the constitutive relations are in turn
quantified in 3.1 to 3.6. The geometric features of the
deforming body are expressed in terms of the coordinate
variables in equations 3.8 to 3.11. To model the pipette
aspiration of a cortical shell, all the above equations have to
be accounted for over the entire surface at any instant of time.
For a general constitutive model, it is not surprising that only
approximate solutions can be obtained by numerical means.
However, a closed form solution does exist in the case of
membranes with no resistance (static or dynamic) to in-plane
shear. Here, because the shear resultant vanishes, the portion
of the cell exterior to the pipette must remain spherical (see
equation 3.14b). It follows that the isotropic tension, and
hence α, is uniform over the deforming surface at any time. A

detailed outline of the solution to this isotropic problem is given in appendix B. These results can be used to verify the validity of the numerical approach to the more general case, where the shear viscosity and the shear elasticity can be non-zero.

We will now describe the numerical method for solving the general cortical shell problem with both isotropic and in-plane shear resultants. Here, the time evolution of the flow process is approximated by a series of small displacements, each over a short time interval Δt. At each time step, the viscous component of the constitutive relation is treated "quasi-elastically" by dividing the viscous moduli by Δt. The resulting solution, in the form of a displacement field, is then added to the original geometry to approximate the cell shape at the end of the time interval. Let the shape at time t be specified by cylindrical coordinates (r,z), and that at time $t+\Delta t$ by (r',z'). The incrementing functions are defined as

$$\Delta r(s_o) \equiv r' - r \tag{3.33a}$$

$$\Delta z(s_o) \equiv z' - z \tag{3.33b}$$

All geometrically related variables (eg: λ_m, $\sin \theta$, R_m, etc) can now be written in the same manner; ie: for any such quantity x, let x' be its value at time $t+\Delta t$, x be the value at t, and

$$\Delta x \equiv x' - x$$

In general, Δx can be expanded in a Taylor series in terms of Δr and Δz. For small Δt, the problem is <u>linearized</u> by truncating the series after the first powers.

The rates of strain are approximated by dividing the increments by Δt. For example, the dilatory strain rate , which was previously written as

$$V_\alpha \;=\; \frac{1}{1+\alpha}\,\frac{\partial \alpha}{\partial t}$$

can now be approximated by

$$V_\alpha \;\approx\; \frac{\Delta\alpha}{(1+\alpha)\Delta t}$$

where $\Delta\alpha$ is linear in $\Delta r(s_o)$ and $\Delta z(s_o)$. With these approximations, constitutive relations that involve viscosities now become quasi-elastic. For instance, let $\bar{T}'$ be the isotropic tension in a Voigt material at time $t+\Delta t$, then

$$
\begin{aligned}
\bar{T}' &= K\,(\alpha + \Delta\alpha) \;+\; \kappa\,V_\alpha \\
&= K\,\alpha \;+\; \left[\, K + \frac{\kappa}{(1+\alpha)\Delta t} \,\right]\Delta\alpha \\
&\equiv \bar{T} \;+\; \Delta\bar{T}
\end{aligned}
$$

where $\bar{T} = K\alpha$ is the cumulated elastic stress up to time t, and $\Delta\bar{T} \equiv \left[K + \frac{\kappa}{(1+\alpha)\Delta t}\right]\Delta\alpha$ is the increment in stress resultant (also linear in Δr and Δz) due to perturbation in geometry. The effective elastic modulus is $K + \frac{\kappa}{(1+\alpha)\Delta t}$, which, for small Δt, is dominated by the quasi-elastic term.

We see that the numerical scheme is a systematic way of writing all quantities in terms of their values at time t, plus an incremental amount due to geometric perturbation over a time interval Δt. The increments are linearized to contain only the first powers of the basic perturbation functions $\Delta r(s_o)$ and $\Delta z(s_o)$. The residual functions, as defined in equations 3.14, are also written in the same manner:

$$\epsilon_\alpha{}' \equiv \epsilon_\alpha + \Delta\epsilon_\alpha = 0 \qquad (3.34a)$$

$$\epsilon_s{}' \equiv \epsilon_s + \Delta\epsilon_s = 0 \qquad (3.34b)$$

These are the equations of mechanical equilibrium that must hold everywhere on the cell surface. Note that by requiring the primed quantities be zero, we are satisfying the force balance condition in the perturbed geometry. Here lies the reason for using the linear quasi-elastic approach: For the pipette aspiration of a spherical shell (ie: the starting geometry) with non-zero shear viscosity, there is no solution consistent with the volume conservation requirement. To avoid violating the incompressibility condition, the equilibrium equations must be applied to a slightly perturbed sphere. This perturbation, however, is not arbitrary since it defines an average velocity field in the time interval Δt, from which the viscous stresses are calculated.

The object of the quasi-elastic approach is to obtain incrementing functions (Δr and Δz) for the entire cell surface. This is done by seperating the cell into two regions: For the portion exterior to the suction pipette, equations 3.34 are used to solve for the two functions $\Delta r(s_o)$ and $\Delta z(s_o)$. The method to do this will be discussed in the next section. The problem inside the pipette is much simpler because $\Delta r=0$. Further, it can be seen from equation 3.7a that the axial tension is uniform along the tube. There is therefore only one force balance equation (in the axial direction) from which $\Delta z(s_o)$ can be evaluated. The two solutions are matched at the pipette entrance, subject to the constraint of volume conservation. The cell shape (r,z) at time t is then incremented and the procedure is repeated again. In this manner, the viscous flow is approximated by a series of small quasi-elastic displacements.

3.5: IMPLEMENTATION OF NUMERICAL METHOD

So far, all the variables we have introduced (eg: tensions, curvatures, extension ratios, etc.) are continuous in space. Because the problem is axisymmetric, they can be written as functions of the instataneous curvilinear distance s alone. An alternative approach, known as the Lagrangian formulation, is to express all quantities (including s itself) in terms of the initial, time-independent curvilinear distance s_o. This can be done because "mapping" between the instantaneous space and the initial space are assumed to be one-to-one. The next step is to

discretize the s_0 space into a number of grid points. All
continuous functions will now be represented by a series of
nodal values located along the meridional curve. A first
derivative with respect to s_0 is approximated by dividing the
difference between two adjacent nodal values by the local grid
size. Such is the simplest form of numerical differentiation
called the forward-difference formula. In dealing with
curvatures, it is necessary to evaluate second derivatives of
the coordinate variables. These quantities can be represented
by applying the forward difference formula to the first
derivatives of the variables. Additional equations are then
needed to approximate the first derivatives themselves. Thus,
by restricting all derivatives to be at most first order (at the
expense of additional equations), we can cast the two
equilibrium equations (eqns. 3.34) into a <u>finite difference</u> form
that involve nodal values of only two neighboring points. As
will be summarized in appendix C, there are four FDEs (finite
difference equations) in total: two from equations 3.34 and two
to represent the first derivatives of Δr and Δz. The four
unknowns at each node are Δr, Δz, $\frac{\partial}{\partial s_0} \Delta r$ and $\frac{\partial}{\partial s_0} \Delta z$. Because the
FDEs are written between two neighboring points, locally there
are four equations that involve eight unknowns (four nodal
values at each point). Futher, because the equations are linear
in the incrementing functions Δr and Δz, they can be put into a
matrix form. For a grid of N points, there will be N-1 sets of
four algebraic equations in eight unknowns. These equations can
be solved globally if the four boundary conditions (the number

of boundary conditions must equal the number of FDEs) are put
in. The matrix organization for a general set of M difference
equations is shown in figure 10. For clarity, this is done for
a grid with only three nodes, although in the actual
implementation, N is typically several hundred. N_c is the
number of boundary conditions at the first node, and N_s is that
for the end node. The condition of

$$N_c + N_s = M$$

is required for a unique solution. In our case, M=4 and N can
be as large as 500. It is obviously impractical to solve a set
of 2000 linear equations by Gaussian elimination or by any other
direct means. Appendix D describes a method, due to Press et
al. (1986), that takes full advantage of the sparsity of the
matrix in figure 10. Subroutines coded in FORTRAN language that
implement these methods will also be given.

3.6: RESULTS AND DISCUSSION

The quasi-elastic method can be applied to any shell
material model discussed in section 3.3. As a first step, the
flow behaviour of a liquid shell will be investigated. The
algorithm is set up for the constitutive relations given in
equations 3.19 and 3.20, where χ and η are the viscous
parameters. By normalizing with the following three quantities:
the dilatory viscosity χ, the suction pressure P, and the
pipette radius R_p, the problem has only two dimensionless
parameters. They are η/χ and R_p/R, where η is the deviatoric

$$\begin{bmatrix} \boxed{N_c \times M} \\ \quad\boxed{M \times 2M} \\ \qquad\boxed{M \times 2M} \\ \qquad\quad\boxed{N_s \times M} \end{bmatrix} \begin{bmatrix} \vec{x} \end{bmatrix} = \begin{bmatrix} \vec{b} \end{bmatrix}$$
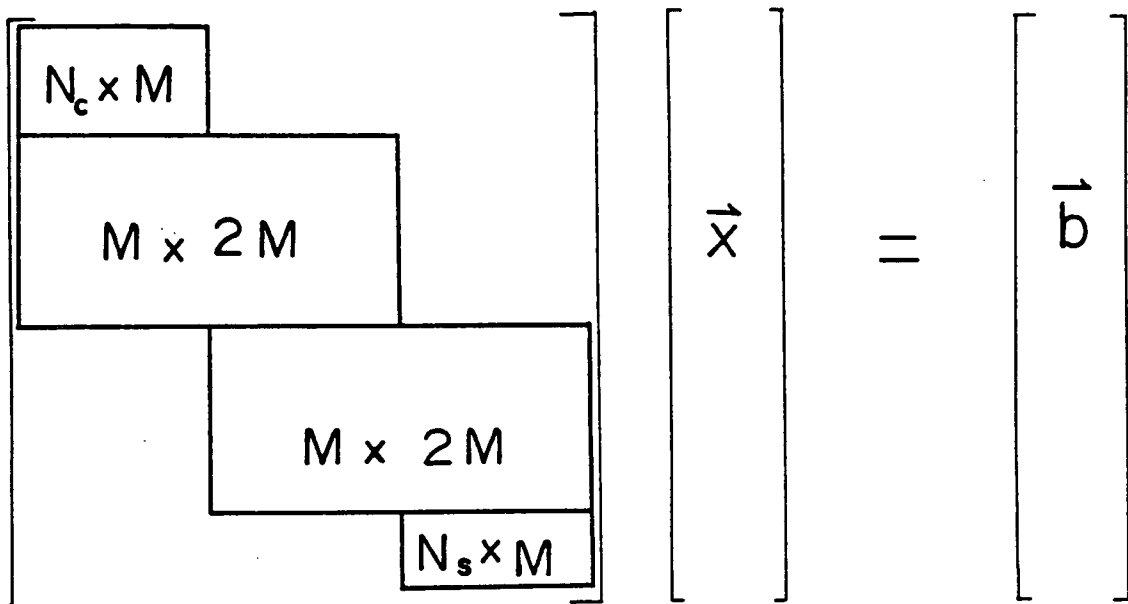
Figure 10: Global matrix structure for a set of M finite-difference equations. The dimensions of each block are as labelled. For simplicity, this is done for a grid with only three nodal points. Matrix elements that lie outside of the blocks are zeros.

viscosity and R the initial cell radius. The validity of the numerical method is then checked by comparing the results with that of the analytical solution for the case $\eta = 0$ (see appendix B). Figure 11 shows the time evolution of the cell projection inside the tube for two different pipette radii. The instantaneous velocity fields are shown in figure 12. These plots clearly show the agreement of the results obtained by three entirely different means (the analytical results actually involve two methods). Another feature of the numerical method not shown here is the that by setting $\eta / \varkappa$ to zero, the cell shape remains perfectly spherical, even after 30 to 40 time steps. It is also interesting to look at how the initial flow rates vary with pipette radius, as shown in figure 13 for different values of $\eta / \varkappa$. Note that in order to be consistent with actual data reduction, which is plotted as $\dot{L}/R_p$ vs. R_p/R, we are normalizing the flow rates with a time constant defined as

$$\tau = \frac{\varkappa}{P\,R}$$

since it is the cell radius R that remains unchanged as the parameter R_p/R varies. From this plot, it is evident that very small shearing stresses can have large effects on the overall flow rates. The cell shapes are also strongly affected by the shear viscosity, as shown in figure 14 for $R_p/R = 0.4$. It is seen from these computed shapes that cell flattening towards the pipette is indicative of the presence of shearing stresses.
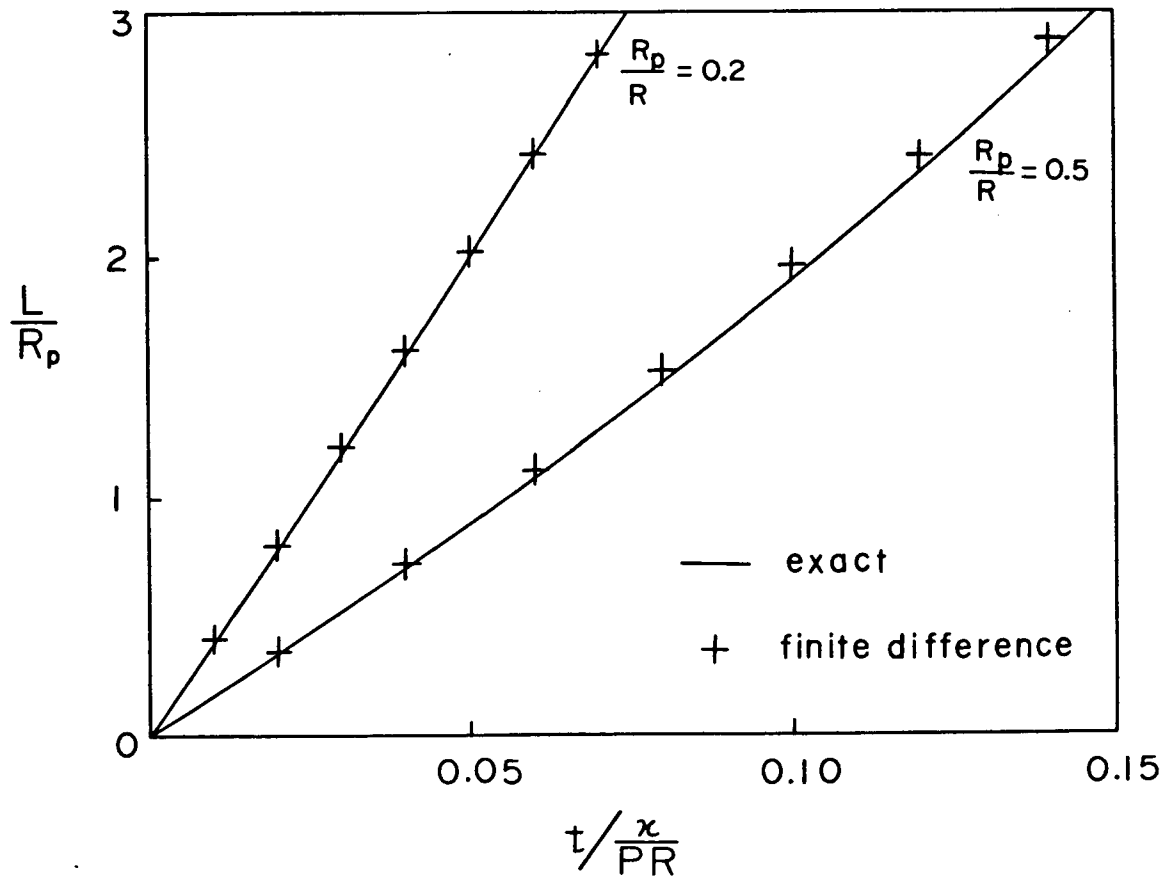
Figure 11: Comparing numerical results to the analytical solution of the time evolution of a surface flow process.
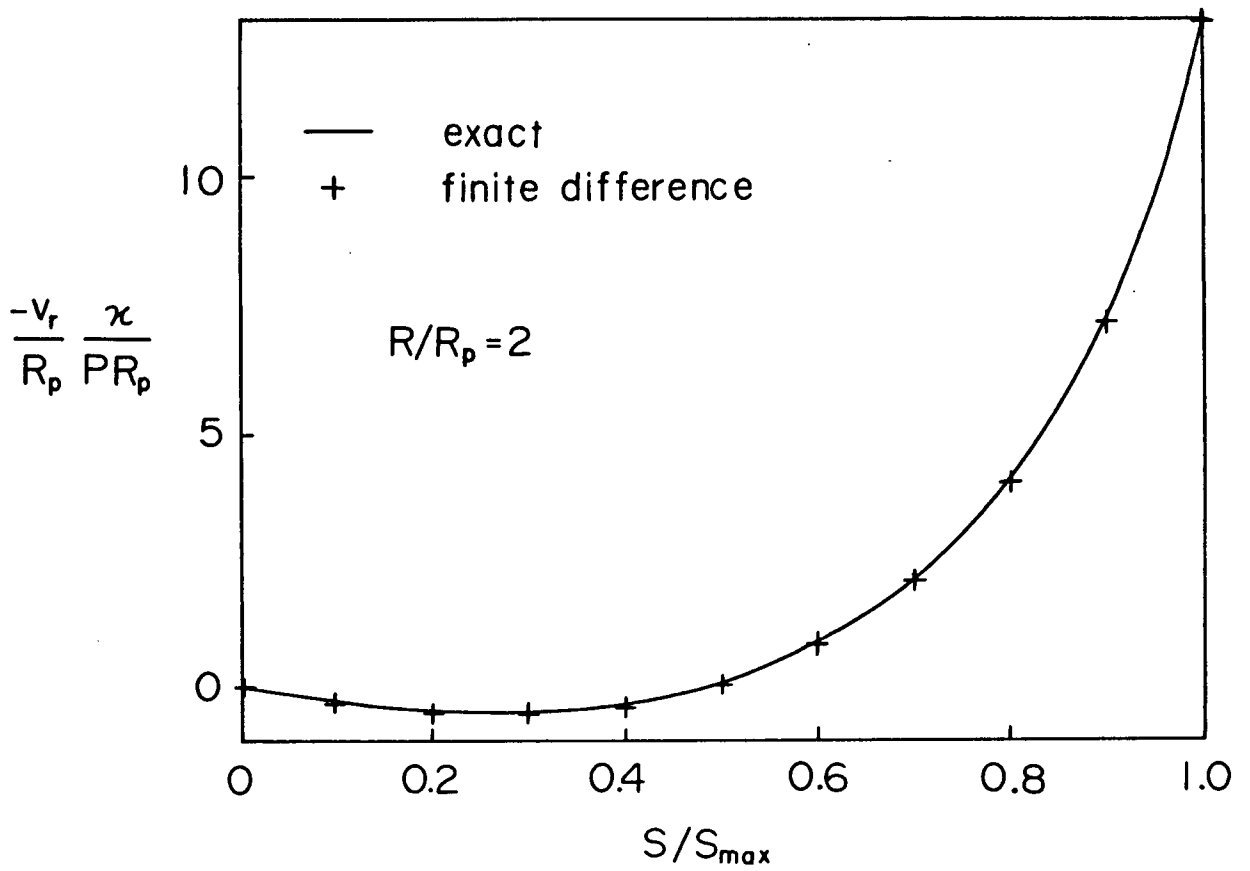
Figure 12(a): Comparing the numerically calculated radial
velocity field to the analytical solution.
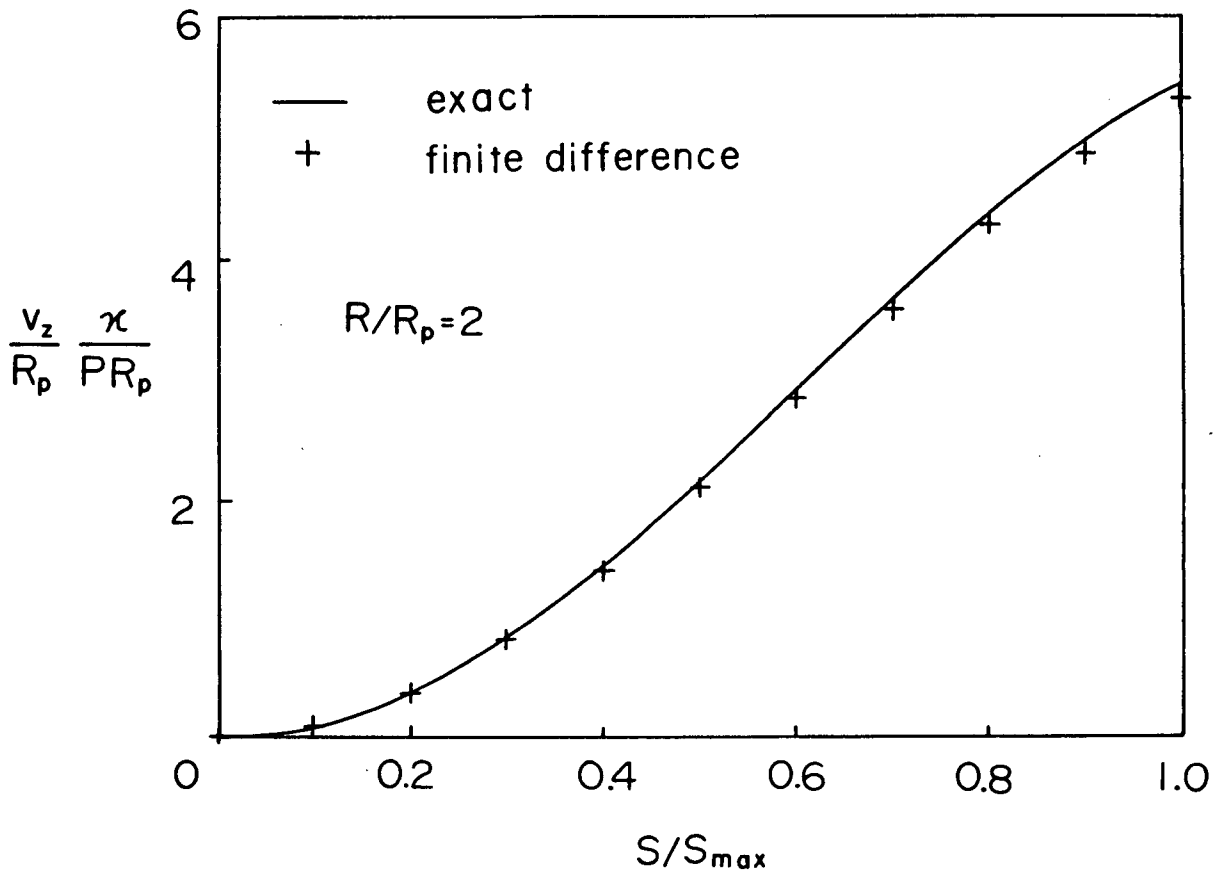S_{max} is the position at the pipette entrance.

Figure 12(b): Comparing the numerically calculated axial velocity field to the analytical solution. S_{max} is the position at the pipette entrance.
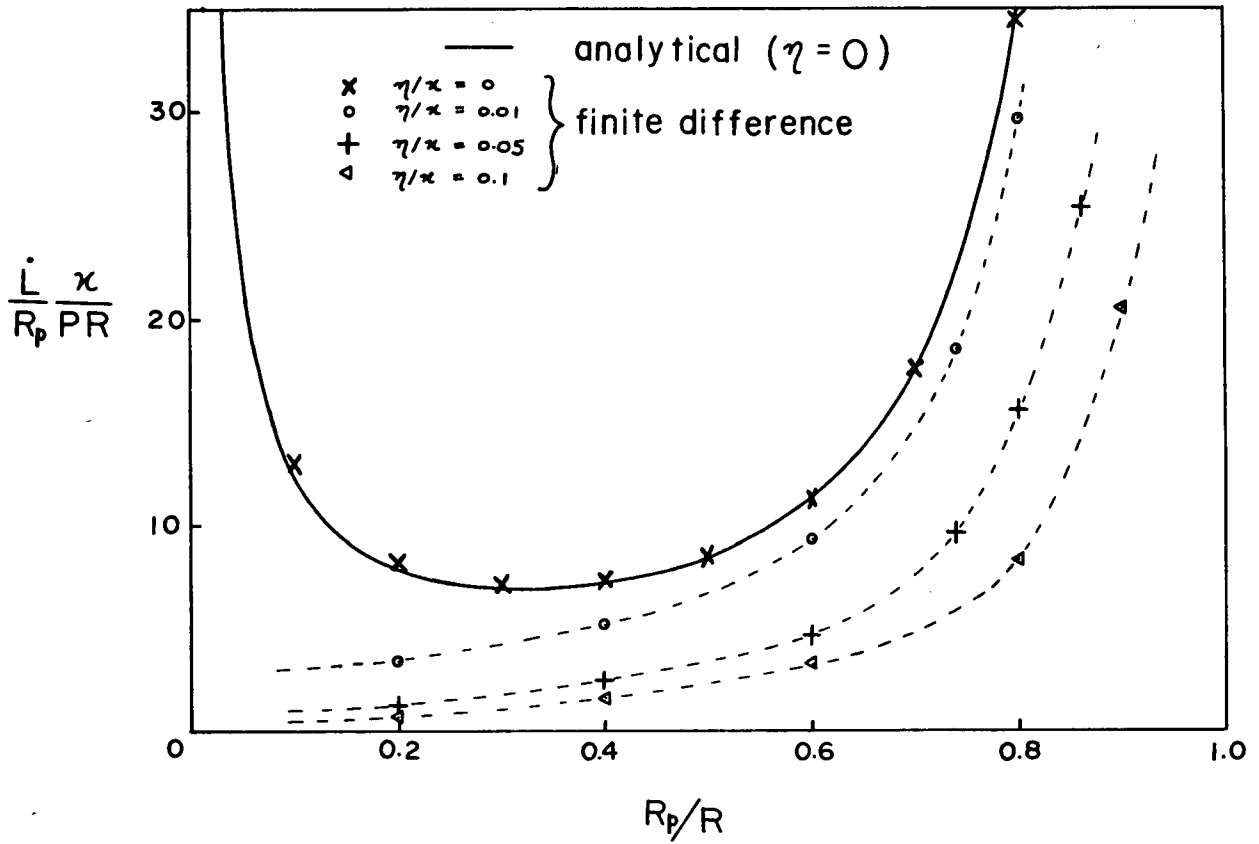
Figure 13: The initial in-flow rate is plotted as a function of the dimensionless pipette radius for several values of $\eta/\varkappa$.
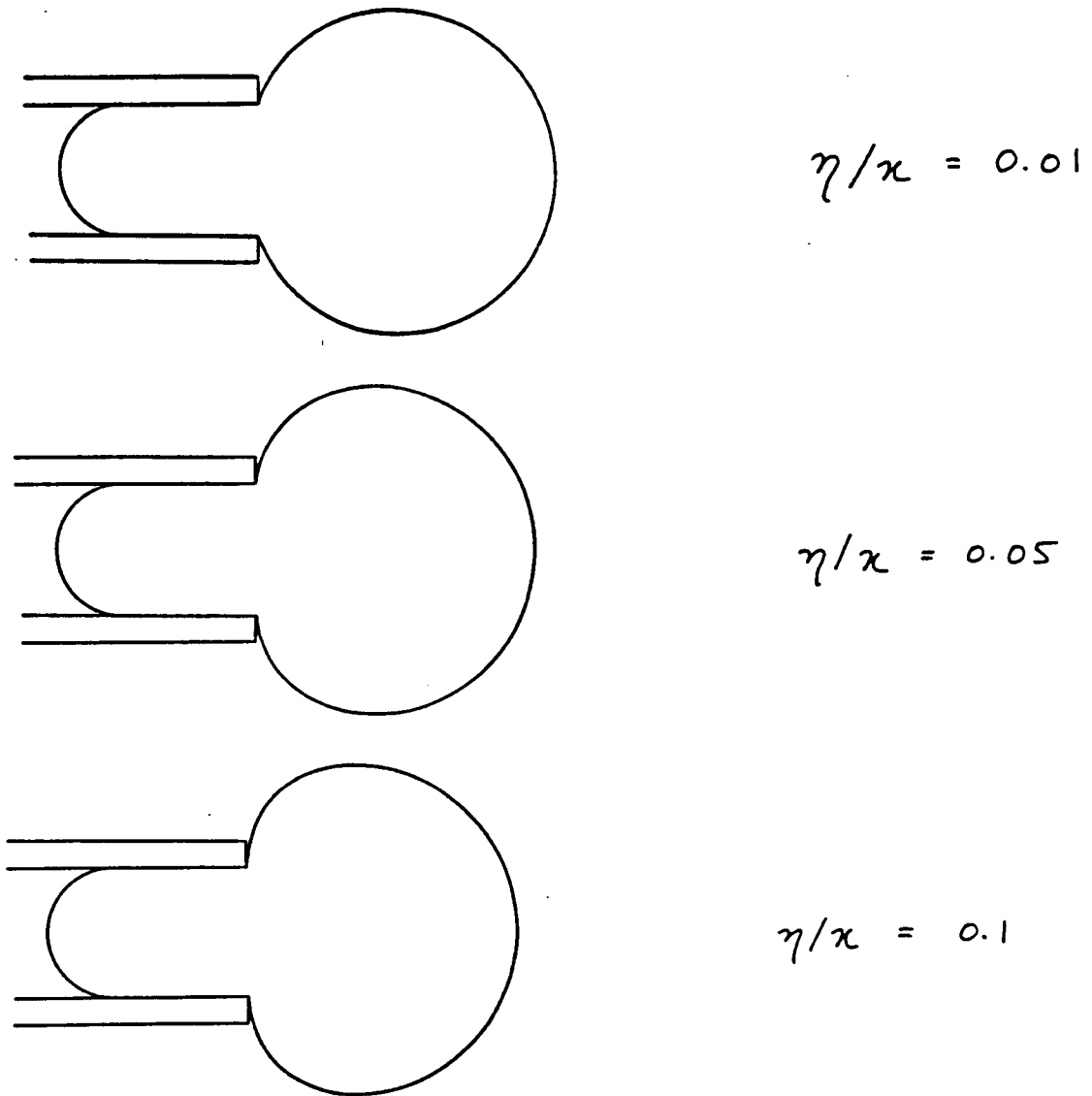
$$\eta/x = 0.01$$

$$\eta/x = 0.05$$

$$\eta/x = 0.1$$

Figure 14: Cell shapes predicted by the numerical method for various values of η/x. The initial cell radius is 2.5 R_p, and the cell projections are 3 R_p in all three cases.

IV. SUMMARY AND DISCUSSION

The work in this thesis is an attempt to better understand
the pipette aspiration of a liquid body with a differentiated
cortical shell in the low Reynolds number situation. Although
presented as a mathematical problem, the analysis is motivated
by our investigation into the mechanical properties of
granulocytic white blood cells. As mentioned in the
introduction, because these cells do not show any elastic limit
to deformation, they can be treated, to first order, as liquid
bodies. Based on biological considerations, one anticipates two
possible regions in which different levels of viscous
dissipation may occur: they are in the cell periphery and in the
interior. Two continuum mechanical problems are posed that
model the cell as having its viscous dissipation dominated
entirely in each of the two regions. Only first order
constitutive relations are used in both cases. These are
equations that relate the viscous stresses to the rates of
deformation by a constant of proportionality. For the interior
model, this amounts to solving the familiar creeping motion
equations in a sphere subject to prescribed stress boundary
conditions. Notable results are the variation in flow rates as
a function of pipette radius as shown in figure 5, and the fact
that the net pressure drop is concentrated in the vicinity of
the orifice entrance. As such, flow rates into the tube will be
insensitive to the geometry of the segment exterior to the
pipette - implying the possibility of representing the flow

process as a pressure drop at the pipette entrance that is proportional to the in-flow rate. In solving the droplet problem, viscous dissipation (and hence the pressure drop) inside the suction pipette is neglected. This assumption, although appears reasonable based on experimental observation (ie: the fact that the cell slides freely on the pipette wall), should be examined critically especially in cases of membrane driven flows. This can be done by solving the creeping motion equations inside the cylinder with either stress- or velocity-boundary conditions on the surface adjacent to the pipette wall.

The cortical model is fundamentally different from the droplet model because energy dissipation is confined within the surface plane. By neglecting bending moments in the cortical layer (as justified by the sharp bend around the pipette edge in figure 1), the tension resultants must act tangent to the deforming surface, thus simplifying the equations of mechanical equilibrium considerably. These equations are solved by a quasi-elastic numerical method which accounts for the viscous stresses both inside and external to the suction pipette. Satisfactory agreement is obtained between the numerical results and the analytical solution for the case $T_s = 0$ (see figures 11,12,13). The numerical procedure is then extended to flow situations where shear viscosity can be non-zero. A kinematic consequence of surface flow into a tube is that very large magnitudes of in-plane shear occur (ie: squares become highly extended rectangles), especially in regions near the pipette

entrance. This is reflected in the significant changes in flow
rates with the introduction of very small values of shear
viscosity into the constitutive relations, as shown in figure
13.

The flow rates in figure 5 and 13 are normalized to be
consistent with actual data reduction, which is plotted as
$d(L/R_p)/d(t\Delta P)$. In comparing the two theoretical plots, it is
evident that the entry flow rates for the droplet model has less
variation with pipette radius. This may be attributed to the
loaclization of the viscous dissipation region near the orifice
entrance, which, for small values of R_p/R, becomes insensitive
to the external boundaries. It is therefore possible to
identify the dominant region of viscous dissipation by
performing aspiration tests with different sized pipettes. This
information can be combined with ultrastructural evidence in
creating a more complete picture of biological cells.

APPENDIX A: SOLUTION TO CREEPING MOTION EQUATIONS

In this appendix, we propose to solve the creeping flow equations

$$\nabla^2 (\vec{\nabla} \times \vec{v}) = 0 \qquad (2.10)$$

in the case of a spherical newtonian droplet subject to the stress boundary conditions

$$\sigma_{\rho\rho}(\zeta)\Big|_{\rho=R} = \alpha(\zeta) \qquad (2.12)$$

$$\sigma_{\rho\theta}(\zeta)\Big|_{\rho=R} = 0 \qquad (2.13)$$

The applied stress $\alpha(\zeta)$ is defined as

$$\alpha(\zeta) = \begin{cases} \Delta P ; & -1 < \zeta < \zeta_p \\ -\lambda/\epsilon ; & \zeta_p < \zeta < \zeta_p+\epsilon \\ 0 ; & \zeta_p+\epsilon < \zeta < 1 \end{cases} \qquad (2.11)$$

which represents a pipette suction pressure. The general axisymmetric solution to equation 2.10 is developed by Happel and Brenner (1973). In spherical components, the velocity fields are given by

$$v_\rho = -\sum_{n=2}^{\infty} (A_n \rho^{n-2} + C_n \rho^n) P_{n-1}(\zeta) \qquad (A.1)$$

$$v_\theta = \sum_{n=2}^{\infty} \left[n \, A_n \, \rho^{n-2} + (n+2) \, C_n \, \rho^n \right] \frac{I_n(\zeta)}{\sin \theta} \qquad (A.2)$$

where the constants A_n and C_n are arbitrary. $P_n(\zeta)$ is the Legendre polynomial of degree n, and $I_n(\zeta)$ is the Gagenbaur polynomial given by equation 2.15. By combining this solution with equation 2.9, an expression for the pressure field is obtained. Since 2.9 involves the gradient of p, the pressure distribution can only be determined up to an additive constant (say π):

$$p = -\eta \sum_{n=2}^{\infty} \left[\frac{2(2n+1)}{n-1} \, C_n \, \rho^{n-1} \right] P_{n-1}(\zeta) + \pi \qquad (A.3)$$

The viscous stresses can be expressed in terms of the pressure and velocity fields according to eqn. 2.6, which is written in tensor form. In terms of spherical polar coordinates, we have (see Landau and Lifshitz, 1982)

$$\sigma_{\rho\rho} = -p + 2 \eta \frac{\partial v_\rho}{\partial \rho} \qquad (A.4)$$

$$\sigma_{\rho\theta} = \eta \left(\frac{1}{\rho} \frac{\partial v_\rho}{\partial \theta} + \frac{\partial v_\theta}{\partial \rho} - \frac{v_\theta}{\rho} \right) \qquad (A.5)$$

By substituting A.1 and A.1 into A.5, and using the identity

$$\frac{dP_{n-1}(\zeta)}{d\theta} = -n(n-1) \frac{I_n(\zeta)}{\sin \theta} \qquad (A.6)$$

the free-slip boundary condition (eqn. 2.13) becomes

$$2n(n-2) \ R^{n-3} \ A_n \ + \ 2(n^2-1) \ R^{n-1} \ C_n \ = \ 0 \ ; \quad n \geq 2 \qquad (A.7)$$

For n=2, we must have

$$C_2 \ = \ 0 \qquad\qquad (A.8)$$

while A_2 can be arbitrary.

In a similar fashion, we substitute equations A.1 ,A.3 into A.4 and equate to the external normal stresses according to 2.12. The resulting expression is

$$\sum_{n=2}^{\infty} \left[2(n-2) \ R^{n-3} \ A_n \ + \ \frac{2n^2-6n-2}{n-1} \ R^{n-1} \ C_n \right] P_{n-1}(\zeta)$$
$$= \ - \frac{1}{\eta} \left[\Pi \ + \ \alpha(\zeta) \right] \qquad (A.9)$$

The right hand side of A.9 can be expanded as a sum of Legendre polynomials with coefficients a_n:

$$\sum_{n=1}^{\infty} a_n \ P_{n-1}(\zeta) \ \equiv \ - \frac{1}{\eta} \left[\Pi \ + \ \alpha(\zeta) \right] \qquad (A.10)$$

Using the orthogonal property, the coefficients a_n are given by

$$a_n \ = \ - \frac{1}{\eta} \ \frac{2n-1}{2} \ \int_{-1}^{1} \left[\Pi \ + \ \alpha(\zeta) \right] \ P_{n-1}(\zeta) \ d\zeta \qquad (A.11)$$

The series in A.9 excludes terms associated with n=1 to avoid infinite velocities at the poles. Accordingly, a_1 must be set

to zero. This results in the expression

$$2\Pi + \Delta P(1+\zeta_p) - \lambda = 0 \qquad \text{(A.12)}$$

Also, because $C_2=0$, we see from A.9 that a_2 has to vanish as well. This is in fact equivalent to the balance of axial forces on the spherical body, which leads to the equation

$$\lambda = \Delta P \, \frac{\zeta_p^2 - 1}{2\zeta_p + \epsilon} \qquad \text{(A.13)}$$

Combining equations A.12 and A.13, the integration constant Π can be related to the suction pressure ΔP by

$$\Pi = -\frac{\Delta P}{2} \, \frac{(1+\zeta_p)(1+\zeta_p+\epsilon)}{2\zeta_p+\epsilon} \qquad \text{(A.14)}$$

For $n \geqslant 3$, A.11 can be integrated using the relation

$$\int P_{n-1} \, d\zeta = \frac{P_n - P_{n-2}}{2n-1} + c \qquad \text{(A.15)}$$

to obtain

$$a_n = -\frac{1}{2\eta} \left\{ \Delta P \left[P_n(\zeta_p) - P_{n-2}(\zeta_p) \right] \right.$$
$$\left. - \frac{\lambda}{\epsilon} \left[P_n(\zeta_p+\epsilon) - P_{n-2}(\zeta_p+\epsilon) - P_n(\zeta_p) + P_{n-2}(\zeta_p) \right] \right\} \quad \text{(A.16)}$$

The normal stress boundary condition can now be matched at each separate harmonic according to A.9. For $n \geqslant 3$, we have

$$2(n-2) \ R^{n-3} \ A_n \ + \ \frac{2n^2-6n-2}{n-1} \ R^{n-1} \ C_n \ = \ a_n \qquad (A.17)$$

Equations A.17 and A.7 can now be solved simultaneously. In terms of the Legendre coefficients, the constants A_n and C_n are:

$$\left. \begin{array}{l} A_n \ = \ \dfrac{(n+1)(n-1)^2}{2(n-2)(2n^2+1)} \ \dfrac{a_n}{R^{n-3}} \\[4mm] C_n \ = \ - \ \dfrac{n(n-1)}{2(2n^2+1)} \ \dfrac{a_n}{R^{n-1}} \end{array} \right\} \quad n \geq 3 \qquad (A.18)$$

Substituting A.18 back into A.1 - A.3, the final solutions for $\rho = R$ are

$$v_\rho \ = \ - \ A_2 \ \zeta \ - \ \sum_{n=3}^{\infty} \ \frac{(n-1)(2n-1)}{2(n-2)(2n^2+1)} \ R \ a_n \ P_{n-1}(\zeta) \qquad (A.19)$$

$$v_\theta \ = \ A_2 \ \sin\theta \ + \ \sum_{n=3}^{\infty} \ \frac{3n(n-1)}{2(2n^2+1)(n-2)} \ R \ a_n \ \frac{I_n(\zeta)}{\sin\theta} \qquad (A.20)$$

$$p \ = \ \Pi \ + \ \eta \ \sum_{n=3}^{\infty} \ \frac{n(2n+1)}{(2n^2+1)} \ a_n \ P_{n-1}(\zeta) \qquad (A.21)$$

where the arbitrary constant A_2 can be interpreted as an axial velocity superimposed onto the existing velocity field. This is allowed because neither the pressure nor the rate of strain tensor are affected.

APPENDIX B: PIPETTE ASPIRATION OF CORTICAL SHELL IN THE
ABSENCE OF IN-PLANE SHEARING STRESSES

The problem of the aspiration of a liquid membrane can be solved analytically when there are no surface shear stresses. In this case, the constitutive relation is

$$\bar{T} = \kappa\, V_\alpha \qquad\qquad (3.19)$$

while η ,the shear viscosity in equation 3.20, is identically zero. It is important to recognize that since there are no shearing stresses, the cell geometry must remain spherical at all times. There are actually two seperate problems involved, they are: 1) the solution of the instantaneous velocity field for a given geometry, and 2) the time evolution of the cell. These will be dealt with by two different methods.

To obtain expressions for the velocity profile, we first rewrite the dilatory strain rate in terms of the velocity components (see Evans and Skalak, 1980):

$$V_\alpha = \frac{\partial v_s}{\partial s} + \frac{v_s}{r} + v_n \left(\frac{1}{R_m} + \frac{1}{R_\phi} \right) \qquad\qquad (B.1)$$

where v_s and v_n are the tangential and normal velocity components, respectively. Because the cell is spherical with radius R, equation B.1 can be written, using the relation s=Rθ, as

$$V_\alpha = \frac{1}{R \sin \theta} \frac{\partial}{\partial \theta} (v_s \sin \theta) + \frac{2 v_n}{R} \qquad \text{(B.2)}$$

Since the cell is to remain spherical, the normal velocity, relative to the centre of the sphere, must be a constant (say $\dot{R}$). We substitute this, along with equation 3.19 into B.2 to obtain

$$\frac{\partial}{\partial \theta} (v_s \sin \theta) = a \sin \theta \qquad \text{(B.3)}$$

where the quantity

$$a \equiv \frac{\overline{T} R}{\kappa} - 2 \dot{R} \qquad \text{(B.4)}$$

is independent of θ. Equation B.3 can now be integrated to obtain the velocity field. In a reference frame fixed at the centre of the sphere

$$v_s = a \frac{1 - \cos \theta}{\sin \theta} \qquad \text{(B.5a)}$$

$$v_n = \dot{R} \qquad \text{(B.5b)}$$

Using the transformations

$$v_r = v_s \cos \theta + v_n \sin \theta \qquad \text{(B.6a)}$$

$$v_z = v_s \sin \theta - v_n \cos \theta \qquad \text{(B.6b)}$$

the velocity field in B.5 can be rewritten in terms of the radial and axial components. Also, to be consistent with the numerical solution, an axial velocity is added to the velocity field so that the base of the sphere (s=0) remains stationary. The final results are

$$v_r = a \frac{\cos \theta (1 - \cos \theta)}{\sin \theta} + \dot{R} \sin \theta \qquad (B.7a)$$

$$v_z = (a+\dot{R})(1 - \cos \theta) \qquad (B.7b)$$

The two parameters a and $\dot{R}$ are uniquely related if volume conservation is accounted for.

The time evolution of the cell can be expressed as a closed form solution by rearranging equation 3.19:

$$\frac{d\alpha}{dt} = \frac{\overline{T}(1+\alpha)}{\kappa} \qquad (B.8)$$

where $\overline{T}$ and α are both uniform over the deforming surface. The object is to relate $\overline{T}$ to α, and hence integrate equation B.8. Consider an aspirated cell with tounge length L and a spherical segment of radius R, as shown in figure 15. The volume and surface area in this configuration are given by

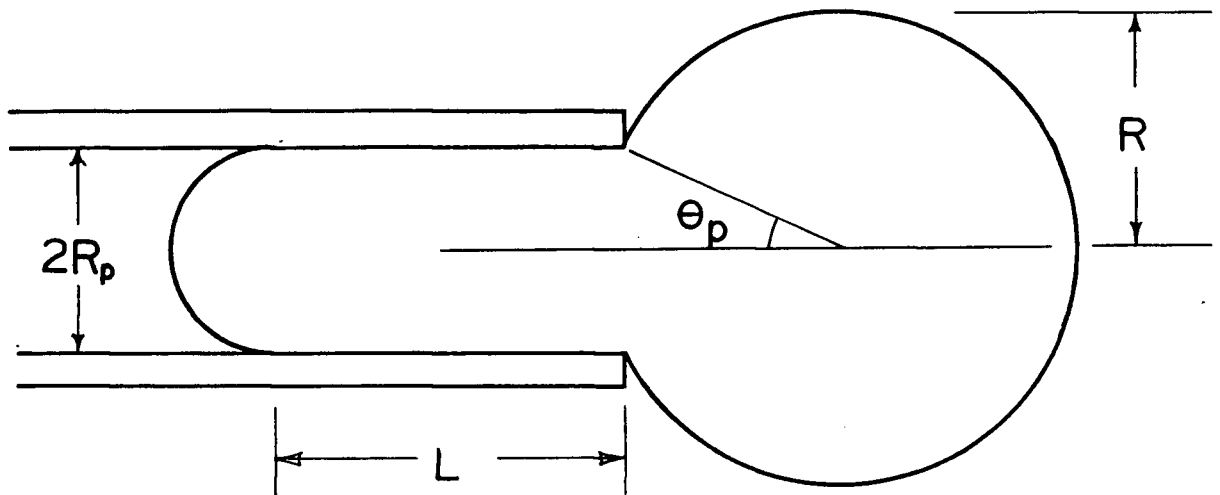$$V = \pi R_p^2 L + \frac{\pi}{3} R^3 (1+\zeta_p)^2 (2-\zeta_p) + \frac{2}{3} \pi R_p^3 \qquad (B.9)$$

Figure 15:   Definition of various dimensions for the problem
posed in appendix B.

$$A = 2\pi R_p L + 2\pi R^2 (1+\zeta_p) + 2\pi R_p^2 \tag{B.10}$$

where

$$\zeta_p \equiv \cos \theta_p \tag{B.11}$$

is a positive quantity. Given V and A, ζ_p can be solved for from the following cubic equation:

$$\frac{1+c^2}{c^2} \zeta_p^3 - 3 \frac{(1+c)^2}{c^2} \zeta_p^2$$

$$+ 3 \frac{(1+c)(3+c)}{c^2} \zeta_p - \frac{(1+c)(5+c)}{c^2} = 0 \tag{B.12}$$

where the quantity

$$c \equiv \frac{6V - 3R_p A}{2\pi R_p^3} + 1 \tag{B.13}$$

for constant volume, is a function of A alone. Thus, given A (or α), we can solve for ζ_p using B.12. The quantities R and L follow immediately:

$$R = R_p / (1-\zeta_p^2)^{\frac{1}{2}} \tag{B.14}$$

$$L + R_p = \frac{A}{2\pi R_p} - \frac{R^2(1+\zeta_p)}{R_p} \tag{B.15}$$

By requiring the meridional tension to be continuous across the pipette entrance, the isotropic tension can be expressed in terms of the suction pressure P and the instantaneous radius R

as

$$\overline{T} = \frac{P\,R_p}{2\,(1 - R_p/R)} \tag{B.16}$$

Since the suction pressure is constant, $\overline{T}$ is only dependent on R. Thus, given the initial cell size (which establishes the total volume) and the instantaneous value of α, we can determine the constant c in B.13. ζ_p is then solved for from equation B.12, from which we can obtain R, L, and $\overline{T}$. In this manner, equation B.8 can be integrated numerically (eg: by the Runge-Kutta method) to very high accuracy.

APPENDIX C: FINITE DIFFERENCE EQUATIONS

A set of four finite difference equations is written between every pair of nodal points. At each node, say node number i ($i=1,2,\ldots,N$, with $i=1$ corresponding to $s=0$), there are four unknowns: $\Delta r(i)$, $\Delta z(i)$, $\frac{\partial}{\partial s_o}\Delta r(i)$, $\frac{\partial}{\partial s_o}\Delta z(i)$. The first two difference equations are to approximate the derivatives of Δr and Δz:

$$\frac{\partial}{\partial s_o}\Delta r(i) = \frac{\Delta r(i) - \Delta r(i-1)}{h_i} \qquad (C.1)$$

$$\frac{\partial}{\partial s_o}\Delta z(i) = \frac{\Delta z(i) - \Delta z(i-1)}{h_i} \qquad (C.2)$$

where i ranges from 2 to N, and h_i is the local grid spacing defined as

$$h_i \equiv s_o(i) - s_o(i-1) \qquad (C.3)$$

The other two difference equations are based on equations 3.34. By expressing the eight unknowns at the two nodes collectively as a_k ($k=1,2,\ldots,8$), equation 3.34 can be rewritten as

$$\frac{\partial}{\partial a_k}\Delta\epsilon_\alpha \cdot a_k = -\epsilon_\alpha \qquad (C4.a)$$

$$\frac{\partial}{\partial a_k}\Delta\epsilon_s \cdot a_k = -\epsilon_s \qquad (C4.b)$$

This is valid because $\Delta\epsilon_\alpha$ and $\Delta\epsilon_s$ are linearized to contain only

the first powers of the solution vector. From the definitions of the residual functions (eqns. 3.14), it follows that

$$\Delta\epsilon_\alpha = 4\Delta\overline{T} + \sigma_n(2R_\phi/R_m - 3)\ \Delta R_\phi + \sigma_n R_\phi^2\ \Delta(\frac{1}{R_m}) \tag{C5.a}$$

$$\Delta\epsilon_s = 4\Delta T_s + \sigma_n(1 - 2R_\phi/R_m)\ \Delta R_\phi - \sigma_n R_\phi^2\ \Delta(\frac{1}{R_m}) \tag{C5.b}$$

The curvatures and their increments are given as follows:

$$R_\phi = \frac{r}{\sin\theta} \tag{C.6}$$

$$\Delta R_\phi = \frac{1}{\sin\theta}\ \Delta r - \frac{r\cos\theta}{\sin^2\theta}\ \Delta\theta \tag{C.7}$$

$$1/R_m = \frac{1}{\lambda_m^3}\ (\frac{\partial r}{\partial s_o}\frac{\partial^2 z}{\partial s_o^2} - \frac{\partial z}{\partial s_o}\frac{\partial^2 r}{\partial s_o^2}) \tag{C.8}$$

$$\Delta(\frac{1}{R_m}) = \frac{-3}{R_m\lambda_m}\ \Delta\lambda_m + \frac{1}{\lambda_m^3}\ \left[\frac{\partial\ \Delta r}{\partial s_o}\frac{\partial^2 z}{\partial s_o^2} + \frac{\partial r}{\partial s_o}\frac{\partial^2 \Delta z}{\partial s_o^2}\right.$$
$$\left. - \frac{\partial\ \Delta z}{\partial s_o}\frac{\partial^2 r}{\partial s_o^2} - \frac{\partial z}{\partial s_o}\frac{\partial^2 \Delta r}{\partial s_o^2} \right] \tag{C.9}$$

For the stresses, the forms of $\overline{T}$ and T_s depend on the particular material model chosen. As a simple example, consider the tension resultant in a liquid (eqns. 3.19-3.20):

$$\overline{T} = 0 \tag{C.10}$$

$$T_s = 0 \tag{C.11}$$

$$\Delta \overline{T} \;=\; \frac{\kappa}{\Delta t} \;(\Delta \lambda_m / \lambda_m \;+\; \Delta \lambda_\phi / \lambda_\phi) \tag{C.12}$$

$$\Delta T_s \;=\; \frac{\eta}{\Delta t} \;(\Delta \lambda_m / \lambda_m \;-\; \Delta \lambda_\phi / \lambda_\phi) \tag{C.13}$$

The tensions $\overline{T}$ and T_s are zero because they represent elastic stresses accumulated up to the present configuration. All the increments introduced above can be expressed in terms of the basic deformation variables using the following relations:

$$\Delta \lambda_m \;=\; \cos \theta \; \frac{\partial \Delta r}{\partial s_o} \;+\; \sin \theta \; \frac{\partial \Delta z}{\partial s_o} \tag{C.14}$$

$$\Delta \lambda_\phi \;=\; \Delta r / r_o \tag{C.15}$$

$$\Delta \theta \;=\; \frac{1}{\lambda_m} \; (\cos \theta \; \frac{\partial \Delta z}{\partial s_o} \;-\; \sin \theta \; \frac{\partial \Delta r}{\partial s_o}) \tag{C.16}$$

$$\frac{\partial^2 \Delta r}{\partial s_o}(i) \;=\; \frac{1}{h_i} \left[\frac{\partial \Delta r}{\partial s_o}(i) \;-\; \frac{\partial \Delta r}{\partial s_o}(i-1) \right] \tag{C.17}$$

$$\frac{\partial^2 \Delta z}{\partial s_o}(i) \;=\; \frac{1}{h_i} \left[\frac{\partial \Delta z}{\partial s_o}(i) \;-\; \frac{\partial \Delta z}{\partial s_o}(i-1) \right] \tag{C.18}$$

Since there are four equations, there must also be four boundary conditions to ensure a unique solution. If we choose to locate the reference frame at the base of the cell (s=0), two boundary conditions immediately follow:

$$\Delta r(1) \;=\; 0 \tag{C.19}$$

$$\Delta z(1) \quad = \quad 0 \qquad\qquad (C.20)$$

Also, θ at the base must be always zero. The requirement of $\Delta\theta$ vanishing at s=0 leads to another boundary condition at the first node:

$$\frac{\partial}{\partial s_o} \frac{\Delta z}{}(1) \quad = \quad 0 \qquad\qquad (C.21)$$

At the other end of the grid, a tangential velocity v_s^p can be prescribed. Using the transformation relation

$$v_s \quad = \quad v_r \cos\theta \quad + \quad v_z \sin\theta \qquad\qquad (C.22)$$

the last boundary condition becomes

$$\Delta r(N) \cos\theta \quad + \quad \Delta z(N) \sin\theta \quad - \quad v_s^p \Delta t \quad = \quad 0 \qquad\qquad (C.23)$$

In actual implementation, v_s^p is an iterative parameter that is used to satisfy the volume conservation condition.

APPENDIX D: MATRIX SOLUTION TO FINITE DIFFERENCE EQUATIONS

Figure 10 shows the matrix structure of a typical finite difference scheme, where a system of M differential equations are approximated by difference formulas that involve nodal values of <u>two</u> adjacent points. The method of solution, as outlined by Press et al. (1986), is to reduce the given matrix to a special upper triangular form, as shown in figure 16. To do this, only matrix elements from two blocks need be manupilated at any time. We start with the top N_cxM block in figure 10. This block, along with the first N_c elements on the right hand side, is Gauss reduced until the first N_c columns form an identity matrix. At the end of this process, only the last N_s columns and the corresponding portion of the right hand vector need be stored. This information is then used to eliminate the first N_c columns in the second block, which lies directly underneath the identity matrix. The remaining elements of this block are then Gauss reduced until the next M columns (columns N_c+1 to N_c+M) form an identity matrix. Again, only the last N_s columns, and the corresponding portion of the right hand side are stored. This procedure is repeated until we get to the last block, which has dimensions N_sxM. As before, the first N_c columns are eliminated using information from the previous block. The remaining part of the block is then reduced to an identity matrix, thus attaining the desired form in figure 16. Note that at this stage, only the sub-blocks labelled "S", and the altered right hand side, are stored. From here, the
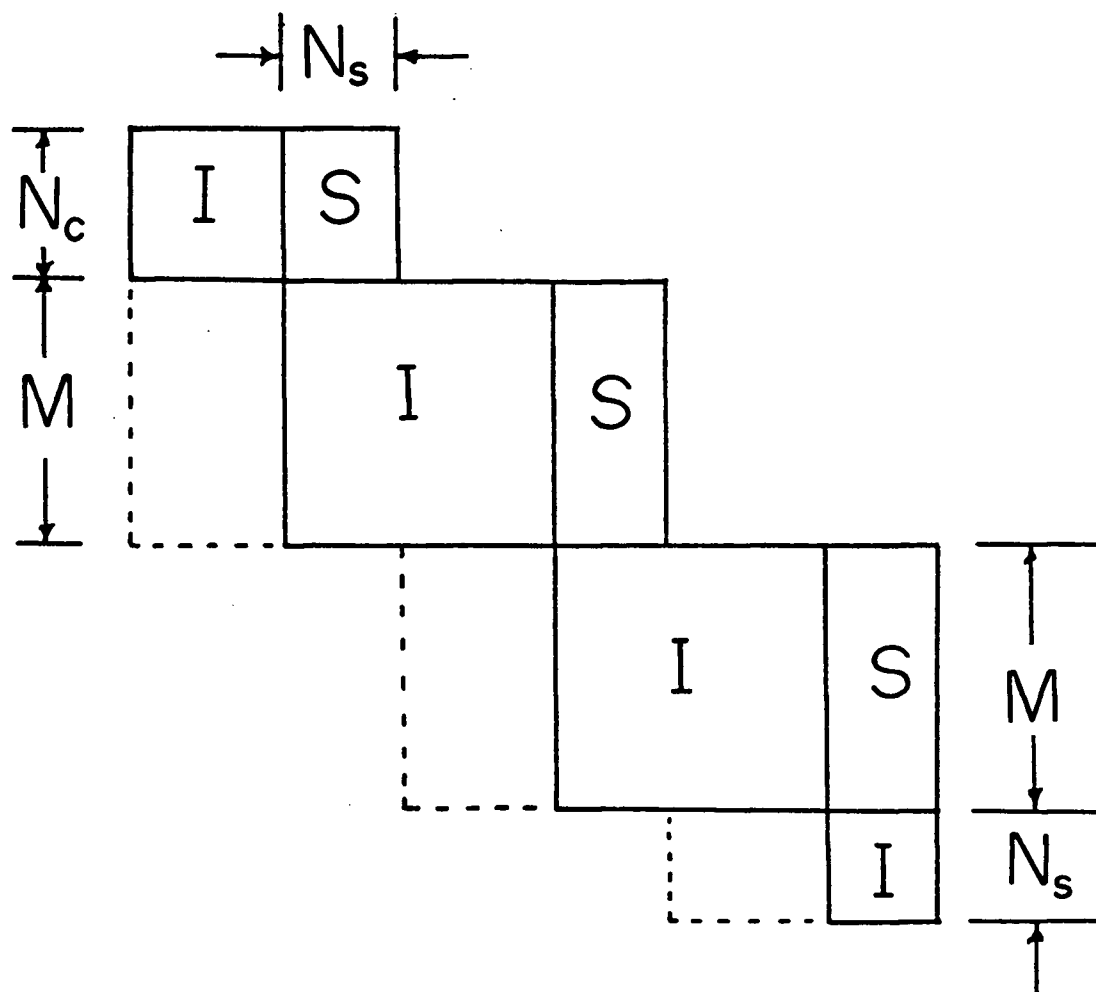
Figure 16: The desired form of the upper triangular matrix which minimizes storage space for the finite-difference solution scheme. Only blocks labelled "S" are stored. The square blocks labelled "I" are identity matrices, and all the remaining entries are zeros.

solution follows quickly by back substitution.

Subroutines coded in FORTRAN are given which implement the above tasks. GJPP performs Gauss-Jordan elimination (with partial pivoting) on a given matrix until an identity matrix is formed. The elimination of the first N_c columns in the sub-blocks is done by subroutine REDUCE. UPTRI is a driver routine which uses GJPP and REDUCE to form the upper triangular matrix shown in figure 16. The user has to supply subroutines BC1, FDE, and BC2, which generate the first (N_cxM), the intermediate (Mx2M), and the last (N_sxM) blocks in figure 10, respectively. The final solution is obtained using BKSUB which perform the necessary back-substitutions.

```
      SUBROUTINE GJPP(A,MA,NA,NC1,IP)
C        Input is matrix A of dimensions MA by NA (NA.GE.MA+NC1).
C        The first NC1 columns are ignored. The rest of the matrix
C        is Gauss reduced (with partial pivoting) until the next
C        MA columns become an identity matrix.
      IMPLICIT REAL*8(A-H,O-Z)
      DIMENSION A(4,9),IP(4),S(4)
      DO 20 I=1,MA
      S(I)=0.
      DO 10 J=1,MA
      IF(DABS(A(I,J+NC1)).GT.S(I)) S(I)=DABS(A(I,J+NC1))
10    CONTINUE
      IF(S(I).EQ.0.D0) GOTO 80
20    IP(I)=I
      DO 70 ID=1,MA
      JD=ID+NC1
      BIG=0.
      DO 30 I=ID,MA
      DUM=DABS(A(IP(I),JD)/S(IP(I)))
      IF(DUM.LE.BIG) GOTO 30
      BIG=DUM
      IMAX=I
30    CONTINUE
      IF(BIG.EQ.0.D0) GOTO 80
      IDUM=IP(ID)
      IP(ID)=IP(IMAX)
      IP(IMAX)=IDUM
      DUM=A(IP(ID),JD)
      IF(DUM.EQ.1.D0) GOTO 45
      DO 40 J=JD,NA
40    A(IP(ID),J)=A(IP(ID),J)/DUM
45    DO 60 I=1,MA
      IF((I.EQ.IP(ID)).OR.(A(I,JD).EQ.0.D0)) GOTO 60
      DUM=A(I,JD)
      DO 50 J=JD,NA
50    A(I,J)=A(I,J)-DUM*A(IP(ID),J)
60    CONTINUE
70    CONTINUE
      GOTO 100
80    WRITE(*,90)
90    FORMAT(' Matrix singular in GJPP, program terminated')
      STOP
100   CONTINUE
      RETURN
      END
C
      SUBROUTINE REDUCE(A,B,NE,NC1,IPT,NPTS)
      IMPLICIT REAL*8(A-H,O-Z)
      DIMENSION A(4,9),B(4,2,510)
      NS=NE-NC1
      IF(IPT.GT.NPTS) GOTO 10
      MA=NE
```

```
        NA=2*NE+1
        GOTO 20
10      MA=NS
        NA=NE+1
20      ID0=NS
        IF(IPT.EQ.2) ID0=0
        DO 50 J=1,NC1
        ID=ID0+J
        DO 40 I=1,MA
        IF(A(I,J).EQ.0.D0) GOTO 40
        DO 30 K=1,NS
30      A(I,NC1+K)=A(I,NC1+K)-A(I,J)*B(ID,K,IPT-1)
        A(I,NA)=A(I,NA)-A(I,J)*B(ID,NS+1,IPT-1)
40      CONTINUE
50      CONTINUE
        RETURN
        END
C
        SUBROUTINE UPTRI(B,NE,NC1,NPTS)
        IMPLICIT REAL*8(A-H,O-Z)
        DIMENSION A(4,9),B(4,2,510),IPIV(4)
        DIMENSION S0(510),R0(510),R(510),Z(510)
        NS=NE-NC1
        NS1=NS+1
        I0=0
        NA=2*NE+1
        NABC=NE+1
        CALL BC1(A,NE,NC1)
        CALL GJPP(A,NC1,NABC,I0,IPIV)
        DO 10 I=1,NC1
        DO 10 J=1,NS1
10      B(I,J,1)=A(IPIV(I),NC1+J)
        DO 30 IPT=2,NPTS
        CALL FDE(A,NE)
        CALL REDUCE(A,B,NE,NC1,IPT,NPTS)
        CALL GJPP(A,NE,NA,NC1,IPIV)
        DO 20 I=1,NE
        DO 20 J=1,NS1
20      B(I,J,IPT)=A(IPIV(I),NC1+NE+J)
30      CONTINUE
        IPT=NPTS+1
        CALL BC2(A,NE,NC1)
        CALL REDUCE(A,B,NE,NC1,IPT,NPTS)
        CALL GJPP(A,NS,NABC,NC1,IPIV)
        DO 40 I=1,NS
40      B(I+NC1,1,1)=A(IPIV(I),NABC)
        RETURN
        END
C
        SUBROUTINE BKSUB(B,NE,NC1,NPTS)
C          Solution X(I) at the J-th grid point is stored in B(I,1,J)
        IMPLICIT REAL*8(A-H,O-Z)
        DIMENSION B(4,2,510),X(2)
```

```
        NS=NE-NC1
        NS1=NS+1
        DO 10 I=1,NS
10      X(I)=B(I+NC1,1,1)
        DO 50 IPTDUM=2,NPTS
        IPT=NPTS+2-IPTDUM
        DO 30 IDUM=1,NE
        I=NE+1-IDUM
        DUM=0.
        DO 20 J=1,NS
20      DUM=DUM+X(J)*B(I,J,IPT)
30      B(I,NS1,IPT)=B(I,NS1,IPT)-DUM
        DO 40 I=1,NS
40      X(I)=B(I,NS1,IPT)
50      CONTINUE
        DO 70 IDUM=1,NC1
        I=NC1+1-IDUM
        DUM=0.
        DO 60 J=1,NS
60      DUM=DUM+X(J)*B(I,J,1)
70      B(I,NS1,1)=B(I,NS1,1)-DUM
        DO 80 I=1,NS
80      B(I+NC1,1,NPTS)=B(I+NC1,1,1)
        DO 90 I=1,NC1
90      B(I,1,1)=B(I,NS1,1)
        DO 120 IPT=2,NPTS
        DO 100 I=1,NS
100     B(I+NC1,1,IPT-1)=B(I,NS1,IPT)
        DO 110 I=1,NC1
110     B(I,1,IPT)=B(I+NS,NS1,IPT)
120     CONTINUE
        RETURN
        END
```

LIST OF REFERENCES

Amato Philip A., Unanue Emil R., Taylor D. Lansing., 1983
Distribution of Actin in Spreading Macrophages: A Comparative
Study on Living and Fixed Cells
The Journal of Cell Biology,96:750-761

Bessis M., 1973
Living Blood Cells and their Ultrastructure
Springer, Berlin

Chein Shu, Sung Kuo-Li Paul, 1984
Effect of Colchicine on Viscoelastic Properties of Neutrophils
Biophysical Journal 46:383-386

Evans Evan A., 1973
A New Material Concept for the Red Cell Membrane
Biophysical Journal 13:926-940

Evans Evan A., Hochmuth R. M., 1977
A Solid-Liquid Composite Model of the Red Cell Membrane
Journal of Membrane Biology 30:351

Evans Evan A., Skalak Richard, 1980
Mechanics and Thermodynamics of Biomembranes
CRC Press, Roca Raton, Florida

Evans Evan A., Kukan B., 1984
Large Deformation, Recovery after Deformation, and
Activation of Granulocytes
Blood 64:1028-1035

Evans Evan A., Needham D., 1986
Physical Properties of Lipid Bilayer Membranes:
Cohesion, Elasticity, and Colloidal Interactions
Journal of Physical Chemistry (submitted)

Fung Y. C., 1965
Foundations of Solid Mechanics
Prentice-Hall, Englewood Cliffs, New Jersey

Happel John, Brenner Howard, 1973
Low Reynolds Number Hydrodynamics
Prentice-Hall, Englewood Cliffs, New Jersey

Kwok R., Evans Evan A., 1981
Thermoelasticity of Large Lecithin Bilayer Vesicles
Biophysical Journal 35:637-652

Landau L. D., Lifshitz E. M., 1982
Fluid Mechanics
Pergamon Press, Oxford

Mitchison J. M., Swann M. M., 1954
The Mechanical Properties of the Cell Surface. I. The Cell
Elastimeter
Journal of Experimental Biology 31:443

Press W. H., Flannery B. P., Teukolsky S. A.,
Vetterling W. T., 1986
Numerical Recipes
Cambridge University Press, Cambridge

Rand R. P., Burton A. C., 1964
Mechanical Properties of the Red Cell Membrane.
Biophysical Journal 4:115

Schmid-Schonbein G. W., Shih Y. Y., Chein S., 1980
Morphometry of Human Leukocytes
Blood 56:866-875

Schmid-Schonbein G. W., Sung K. L. P., Tozeren H.,
Skalak R., 1981
Passive Mechanical Properties of Human Leukocytes
Biophysical Journal 36:243-256

Skalak R., Tozeren A., Zarda R. P., Chien S., 1973
Strain Energy Function of Red Blood Cell Membranes
Biophysical Journal 13:245

Southwick F. S., Stossel T. P., 1983
Contractile Proteins in Leukocyte Function
Seminars in Hematology 20:(4)305-321

Tozeren H., Chein S., Tozeren A., 1984
Estimation of Viscous Dissipation inside an Erythrocyte during
Aspirational Entry into a Micropipette
Biophysical Journal 45:1179-1184